Leibniz Universität Hannover
Institut für Quantenoptik

A Laser System for Gray-molasses Cooling on The D1 Transition of an Atomics Gas of ^{39}K

Submitted by:
Baraa Shammout

in partial fulfillment of the requirements for the degree of
Master of Science
in
Physics

October 2019

Supervisor:
Dr. Alessandro Zenesini

First examiner:
Prof. Dr. Silke Ospelkaus

Second examiner:
apl. Prof. Dr. Carsten Klempt

Declaration

I declare, that the thesis has been authored independently, utilizing no other support than the references and auxiliary means specified. All points in the thesis which have been taken over from other sources, whether literally or analogously, have been marked as such. The thesis has not been submitted to any other examination authority so far, neither in the same nor in a similar form.
Hannover,
2019, Baraa Shammout

Abstract

In this work we present the design and the construction of a laser system for cooling an atomic gas of potassium ^{39}K on the D1-Line by gray molasses technique. The seed laser is an Interference-filter-stabilized external-cavity diode laser (ECDL). The laser frequency is stabilized to one of the atomic features of ^{39}K D1-transition thanks to frequency modulation (FM) spectroscopy. The low seed power is then amplified by means of tapered amplifier (TA). Finally, the cooling and repumping beams are generated and blue-detuned from the atomic transitions $|F = 2\rangle \rightarrow |F' = 2\rangle$ and $|F = 1\rangle \rightarrow |F' = 2\rangle$ using two acousto-optic modulators (AOMs).

Acknowledgement

I would like to thank everyone in our group "AG molecular quantum gases" for their support, guidance and encouragement during one year working on this project, in particular my supervisor Dr. Alessandro Zenesini with his helpful advices and Prof. Dr. Silke Ospelkaus, who gave me the opportunity to join the group.

Contents

List of Figures

List of Tables

Chapter 1

Introduction

Using laser radiation to cool and trap atoms has leaded to a revolution in our approach to investigate fundamental quantum physics and atomic physics. Ultracold atomic gases has become the main tool in studying quantum many body systems [4] since the first observation of Bose-Einstein condensation (BEC) 1995 [7] and Fermi degeneracy 2001 [43] in dilute atomic gases. Potassium, as alkali metal, has attracted much interest in the field of cold atoms because of the existence of both fermionic (^{40}K) and bosonic isotopes (^{39}K,^{41}K). In addition Potassium has broad Feshbach resonances at moderate magnetic fields, which makes possible to tune the particle-particle interactions [8]. Our group is working on creating ultracold bosonic polar molecules of dual species ^{23}N and ^{39}K in the ground state. That would enable us to study dipolar quantum gases to search for novel states of matter like for example "Supersolidity" [31]. Currently, the two atomic gases are pre-cooled separately and then loaded into the science chamber to be cooled and trapped in two-color 3D-magneto-optical trap (MOT), where a sub-Doppler cooling on the D2-transition of ^{39}K is performed in a red-detuned optical molasses. ^{39}K atoms are then sympathetically cooled by ^{23}N atoms, which are cooled by microwave evaporative technique in a magnetic trap and the number of Potassium atoms can be loaded to the magnetic trap is on the order of $10^6 - 10^7$ atoms. The lowst temperature of Potassium atoms have been achieved in our experiment by sub-Doppler cooling on the D2-transition is 106 μK [36]. However, the so-called "recoil limit" of ^{39}K D2-line is $\approx 0.418\mu$K (see [42]). The reason for such inefficient cooling mechanism lies therein that the hyperfine spacing of the D2-line is narrow [16]. In their work, Salomon et.al have demonstrated a new method to cool ^{39}K atoms to further lower temperature [34]. Using the so-called gray molasses cooling [45] on the D1 transition a temperature of 6μK has been achieved. The technique is a combination of two cooling mechanisms, Sisyphus cooling [6] and Velocity Selective Coherent Population Transfer (VSCPT)[1]. So Implementing gray molasses cooling on the D1 transition in addition to D2 would decrease significantly the Potassium temperature and allow us to preserve Sodium atoms which will be not anymore required for the evaporation. Ideally, one could think to load the atoms directly in the dipole trap where the tuning of the scattering length via magnetic Feshbach resonance is possible. That was the motivation for our group to build a laser system to perform gray

molasses cooling on the D1-line of ^{39}K.
This work is organized as follows: chapter 2 introduces the theory of laser cooling, then chapter 3 describes gray molasses cooling on ^{39}K D1 transition. We move on with presenting the experimental setup of the laser system in chapter 4. Finally, we come to the conclusion in chapter 5.

Chapter 2

Principle of laser cooling

According to the equipartition theorem in non-interacting atomic gas the kinetic energy of atom per degree of freedom is equal to its thermal energy [17]

$$\frac{1}{2}k_BT = \frac{1}{2}mv_x^2 \tag{2.1}$$

where:
k_B: Boltzmann constant, T: Temperature, v_x: velocity in one degree of freedom, here is for example in x-axis, m: mass of atom.
Hence the root-mean-square of the thermal velocity is:

$$v_x^{rms} = \sqrt{\frac{k_BT}{m}} \tag{2.2}$$

And in three dimension it can be written as:

$$v_{rms} = \sqrt{\frac{3k_BT}{m}} \tag{2.3}$$

it is obvious that the temperature of an atomic gas is proportional to the velocity square of atoms. Thus, in order to achieve low temperature, velocity of atoms has to be reduced and atoms have to be slowed down.
For a gas of Potassium ^{39}K, $m = \frac{39}{NA}$, the velocity at room temperature T=300K is by calculation then: $v_{rms} = 438$ m/s
Slowing down atoms can be accomplished by using laser light at frequency close to resonance with an atomic transition of atoms of interest. A temperature in the microkelvin range has been achieved by laser cooling with corresponding atom velocity smaller than that at room temperature by about four orders of magnitude [17]. Many laser cooling techniques has been developed over years. In the following sections a brief explanation of these cooling methods is introduced. Starting with Doppler cooling, moving to sub-Doppler cooling, which include Sisyphus cooling and Gray molasses.

2.1 Doppler cooling and scattering force

Considering a given atom with resonance transition ν_0, moving along the x-axis with velocity $+v_x$ and a laser beam propagating in the opposite direction with frequency ν tuned from the resonance frequency ν_0 by δ, so $\nu = \nu_0 + \delta$, where $\delta << \nu_0$ with large detuning ($\delta >>$ Γ linewidth of the atomic transition). Due to Doppler effect the laser frequency seen by atom will be:

$$\nu' = \nu(1 + \frac{v_x}{c}) = (\nu_0 + \delta)(1 + \frac{v_x}{c}) \approx \nu_0 + \delta + \nu_0 \frac{v_x}{c} \tag{2.4}$$

where c: the speed of light in vacuum.
If the detuning δ is belwo the resoncace by the factor v_x/c

$$\delta = -\nu_0 \frac{v_x}{c} = -v_x/\lambda \tag{2.5}$$

then the Doppler shifted frequency will be equal to the atomic resonance $\nu' = \nu_0$. In this case, atom moving in +x direction will absorb a photon of energy $E = h\nu_0$ receiving a momentum kick in the -x direction, re-emitting then light via spontaneous emission and losing that momentum in random direction. The change of momentum by emission averages to zero, while the momentum change of atom by absorption is $\Delta P_x = -\frac{h}{\lambda}$, where λ is the laser wavelength, h: Planck constant. Thus, repeated cycle absorption-emission causes a net loss of momentum in the -x direction, which induces a mechanical force on the atom. The force exert on the atom by light called scattering force (frictional force [17]) and it is given by:

$$F_x = \frac{dP_x}{dt} \approx \frac{\Delta P_x}{2\tau} = -\frac{h}{2\tau\lambda} \tag{2.6}$$

where τ is the transition lifetime.
this frictional force leads to a deceleration defined as:

$$a_x = \dot{v}_x = \frac{F_x}{m} = \frac{\Delta P_x}{2\tau m} = -\frac{h}{2\tau\lambda m} \tag{2.7}$$

and as mentioned before, slowing down atoms means decreasing the temperature. This cooling mechanism is called Doppler cooling.

2.1.1 Optical molasses

Using one single laser beam for cooling is not sufficient, because as atom cooled down the detuning must be reduced [17] until it becomes close to the natural linewidth of the atomic transition ($\delta \approx \Gamma$), in this case atom moving in -x direction will be accelerated instead of decelerated, and hence becoming hotter, by the the scattering force. As an undesired consequence, collision with atoms moving in +x direction will increase the temperature. To overcome this problem a two counterpropagating laser beams should be implemented to form the so-called optical molasses as illustrated in Fig.2.1. In this case atom experiences two different frictional forces from two directions. With this configuration one can cool atoms moving in both directions [17].

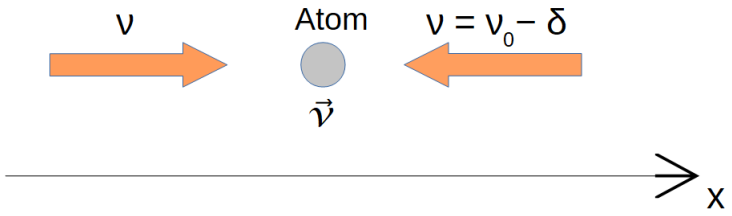

Figure 2.1: Two counterpropagating laser beams at frequency ν detuned by δ below the atomic resonance frequency ν_0 form optical molasses, so atoms moving in both direction +x and -x are involving in the cooling process.

2.1.2 Magneto-optical trap (MOT)

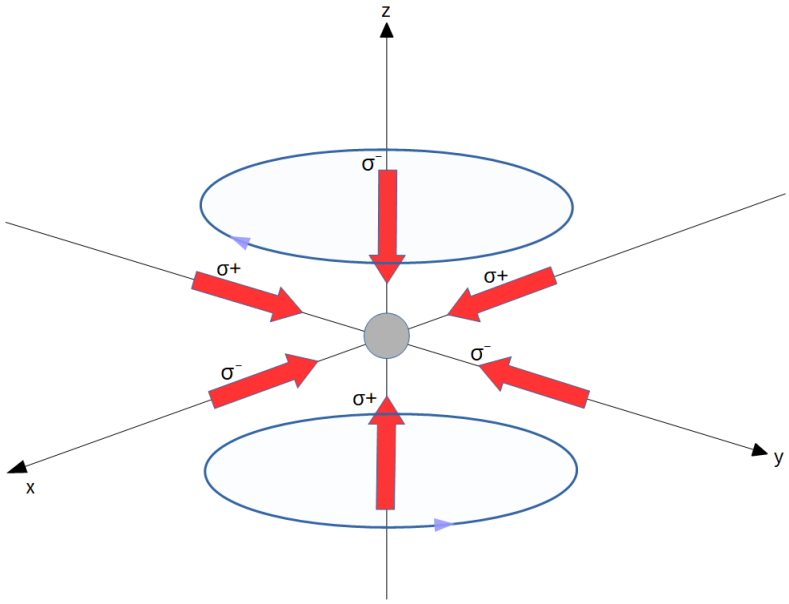

Figure 2.2: Schematic of 3D Magneto-optical trap (MOT), see the text for more details.

One can ask, what about the other dimensions $\pm y$ and $\pm z$? and how to confine atoms locally at one point in the space? The laser cooling arrangement described in the previous section is able to cool atoms only in one dimension wihtout trapping. A more sophisticated technique is required for cooling atoms in three dimensions and for spatial trapping at the same place. This technique is called Magneto-optical trap (MOT). As illustrated in Fig.2.2, six red-detuned counter propagating laser beams with circular orthogonal polarizations form optical molasses in three dimentions providing a confinement in the momentum space and a quadrupole magnetic field $B(z)$, generated by two magnetic coils in an anti-Helmholtz configuration, causes a gradient Zeeman splitting of

the energy levels $E(z)$ given by [15]:

$$E(z) = g_J \mu_B M_J B(z) \tag{2.8}$$

where g_J is Lande g-factor, μ_B Bohr magneton.
Now Considering an atomic gas with resonance frequency ω_0 corresponding to the transition $J = 0 \rightarrow J = 1$ in MOT with laser frequency ω detuned by δ from resonance. Due to Zeeman effect the exited state will split gradually into triplet sub-level excited states $M_J = -1, 0, 1$ as shown in Fig.2.3. So atoms will be always attracted towards the zeropoint at the center of the quadrupole magnetic field, because the Zeeman shift is increasing when moving away from the center and hence the velocity required to be in resonance with the detuned laser is decreasing.

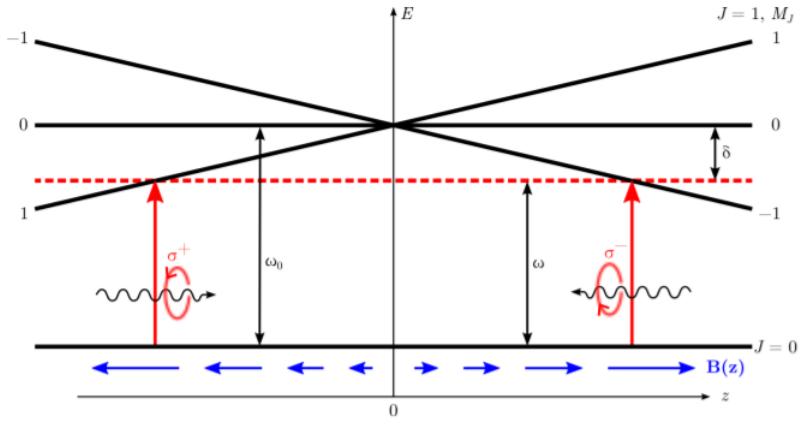

Figure 2.3: Mechanism of the MOT in one dimension for two level atom with resonance frequency ω_0 corresponding to the transition J=0 $\rightarrow$ J=1. Spatial Zeeman splitting of the exited state provides a confinement for atoms in the zeropoint at the center. The frequency ω of the two counter propagating laser beams is red detuned by δ from resonance. The length of the blue arrows represents the strength of the quadrupole magnetic field. Figure from [12]

2.1.3 Doppler limit

By Doppler cooling the atom momentum averages to zero but the mean square doesn't [22], because even the coldest atom can still absorbing and emitting light via random walk. This gives the atom each cycle a momentum, and hence heat. Thus, the velocity can't reach zero. The balancing between heating and cooling defines the lowest achievable temperature, which is limited by the natural linewidth $\Gamma/2\pi$ of the atomic transition

$$\underbrace{k_B T_{min}}_{Thermal\ energy} \sim h\left(\frac{\Gamma}{2\pi}\right) \tag{2.9}$$

T_{min} is the lowest temperature can be achieved by Doppler cooling, which called Doppler limit and it is given by [17]:

$$T_{Doppler} = \frac{\hbar\Gamma}{2k_B} \tag{2.10}$$

the corresponding thermal velocity can be obtained by substitute (2.10) in (2.2)

$$v_x^{min} = \sqrt{\frac{\hbar\Gamma}{2m}} \tag{2.11}$$

for Potassium ^{39}K by cooling on the D1 line $v_x = 17.3$ cm/s

2.2 Sub-Doppler cooling

It's possible to achieve a lower temperature than the Doppler limit given by the equation 2.10 in optical molasses by cooling mechanisms called Sisyphus cooling and Gray molasses, which are explained in the following sections.

2.2.1 Sisyphus cooling (Polarization gradient cooling)

Two counterpropagating laser beams in Lin⊥Lin configuration (orthogonal linear polarizations) interfere creating a standing wave with polarization gradient in a period of $\lambda/2$. The variation of polarization is from σ^+ to linear to σ^-. Now let's assume a two level

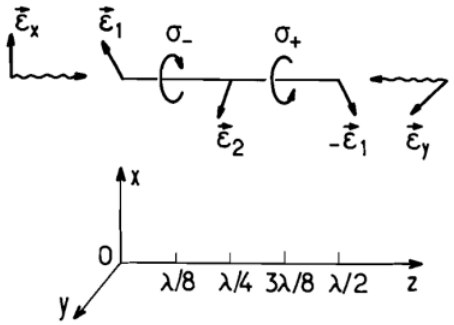

Figure 2.4: Lin⊥Lin configuration shows the polarization gradient in one dimention. Adapted from [6]

alkali atom in a polarization gradient created by laser light with frequency red detuned from the resonance transition $J = \frac{1}{2} \rightarrow J = \frac{3}{2}$. The ground state splits into two states $m_J = -1/2, +1/2$ and the sub-level exited states are described by the magnetic quantum numbers $m_J = -3/2, -1/2, +1/2, 3/2$.
The light shift of energy ΔE is proportional to the square of Rabi frequency Ω_{ge} of

an atomic transition (g denotes the ground state and e denotes the exited state) and inversely proportional to the detuning δ of the laser light.

$$\Delta E \sim \frac{\Omega_{ge}^2}{\delta} \tag{2.12}$$

For red-detuning($\delta < 0$) the light shift of a state is negative and for blue-detuning ($\delta > 0$) the light shift is positive. The Rabi frequency depends specifically on Clebsch-Gordon coefficient C_{ge} of a transition

$$\Omega_{ge} = C_{ge}\Gamma\sqrt{I/2I_{sat}} \tag{2.13}$$

Where Γ is the natural line width of the transition in angular frequency unit, I is the intensity of light, I_{sat} is the saturation intensity (the intensity where the optical Rabi-frequency equals the spontaneous decay rate and it is given by [42]: $I_s = \frac{\pi hc}{3\lambda^3\tau}$).
From the equations 2.12 and 2.13 one can note that the light shift is proportional to the square of the Clebsch-Gordon coefficient, which has different values depending on the allowed transition and the corresponding polarization as illustrated in Fig.2.5 (see the selection rules Table 2.1). Consequently the energy shift of both ground states $m_J = \pm\frac{1}{2}$ is modulated periodically in space with phase shift 180° (Fig.2.6).
Atom moving in along the z-axis experiences a loss in its kinetic energy when climbing the potential hill. If the detuning was taken carefully and atom has reached the top, there will be a high probability to be pumped into the exited state. The atom can then drop to the lower sublevel ground state via spontaneous emission emitting photon with higher energy than the absorbed one, which means having lower kinetic energy and hence lower velocity. If the atom velocity now is high enough to climb the potential, the cycle will be repeated and atom will become colder and colder.

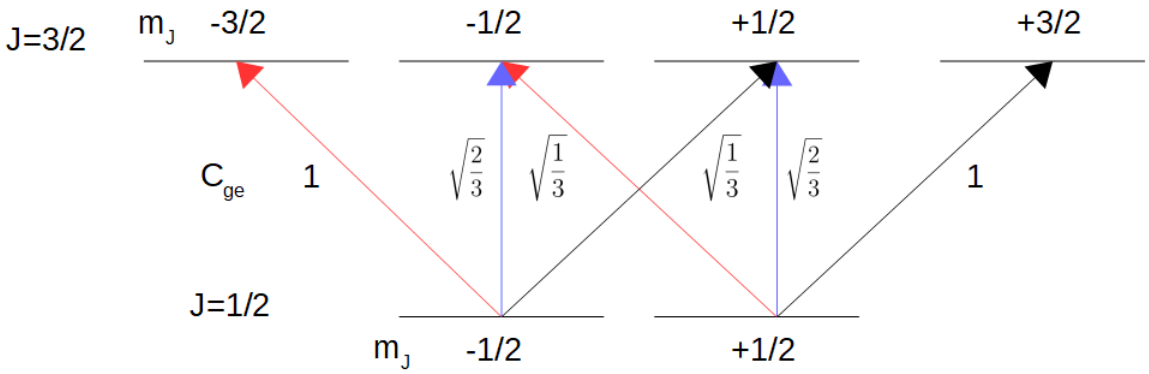

Figure 2.5: Energy sub-levels and the corresponding Clebsch Gordon coefficients of the transition $J = 1/2 \rightarrow J = 3/2$ coupled by light with a linear polarization (blue arrow), σ^+ polarization (black arrow) and σ^- polarization (red arrow). Figure modified after [6], [19]

Allowed transition	Polarization
$\Delta J = 0, \pm 1$ except $J = 0 \rightarrow J' = 0$	$\pi, \sigma^{\pm}$
$\Delta m_J = 0, \pm 1$	
$\Delta F = 0, \pm 1$ except $F = 0 \rightarrow F' = 0$	$\pi, \sigma^{\pm}$
$\Delta m_F = 0, \pm 1$	

Table 2.1: The possible electric dipole transitions in atom with the corresponding polarization [15]

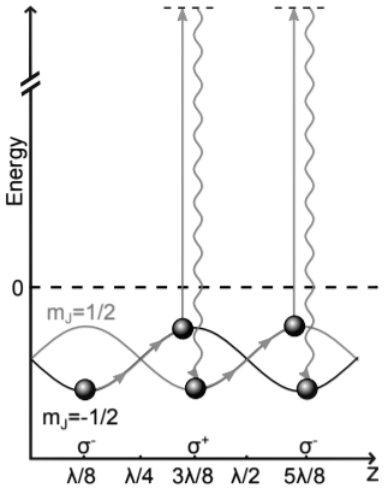

Figure 2.6: Sisyphus cooling scheme for two level atom with ground state J=1/2 and exited state J=3/2. Full explanation can be found in the text. Taken from [40][6].

recoil limit

Even the coldest (slowest) atoms can still absorbing and emitting photons spontaneously. Each time atom emits photon with wavelength λ recoils with momentum $p = \hbar k$, which limits achieving lower temperature. The lowest temperature can be achieved using Sisyphus cooling called the recoil limit. We can obtain the recoil temperature by setting:

$$\text{thermal energy} = \text{kinetic energy of atom}$$

$$k_B T = \frac{p^2}{2m} = \frac{(\hbar k)^2}{2m} \tag{2.14}$$

$$\Rightarrow T_{recoil} = \frac{\hbar^2 k^2}{2m k_B} \tag{2.15}$$

The recoil temperature of ^{39}K D1-line is 0.41436702 μK and the corresponding recoil velocity is about 1.33 cm/s [42]. However, the recoil limit can be broken by a cooling method called gray molasses.

2.2.2 Gray molasses cooling

In principle, gray molasses cooling based on two mechanisms, Sisyphus cooling and Velocity selective coherent population transfer (VSCPT) in present of bright state and dark state of a 3-level atom in gradient polarization with blue detuned light $\delta > 0$ from the atomic resonance. We call a state is bright when it is coupled by light to an exited state. In contrast a dark state is a non-coupled state. The bright state has positive light shift and it is spatial modulated, while the dark state has a flat potential with no light shift. Atom moving in the z-direction climbs the potential of the bright state converting its kinetic energy to potential energy. Once atom reached the potential hill, it can be pumped to the exited state and via spontaneous emission it decays to the dark state undergoes Sisyphus cooling. In this case there are two possibilities, either being coupled again to the bright state or it can be captured and confined in the dark state (see Fig.2.7). This coupling is controlled by the VSCPT mechanism and the probability of the coupling between the dark and bright states is proportional to the atom velocity and inversely proportional to the light shift of the bright state as we will see later. Atom with velocity rather than zero can be always included in the cooling process until reaching zero and be captured by the dark state. In the following section we will see the origin of bright and dark states and understand what Λ-enhanced gray molasses is.

Λ three-level system

Let's introduce a Λ-system (Fig.2.8) with two ground states $|1\rangle$, $|2\rangle$ and exited state $|3\rangle$. The corresponding energies ϵ_1, ϵ_2 and ϵ_3, respectively. The coupling $|1\rangle \rightarrow |3\rangle$ is achieved by light field with frequency ω_1 detuned by δ_1 from resonance and Rabi frequency Ω_1. The coupling $|2\rangle \rightarrow |3\rangle$ is made by light field with frequency ω_2 detuned by δ_2 from resonance and Rabi frequency Ω_2. The relative detuning is $\delta = \delta_1 - \delta_2$.
We can write the Hamiltonain H of a free atom with mass m and momentum p_z as a sum of its kinetic energy and the internal energies assuming that the energy of the ground states is zero and the energy of the exited state $\hbar\omega_3$

$$H = H_{kin} + H_0 = \frac{p_z^2}{2m} + \hbar\omega_3|3\rangle\langle 3| \tag{2.16}$$

The Hamiltonian for the light-atom interaction in the rotating wave approximation can be written as:

$$V = \left(\frac{\hbar\Omega_1}{2}|3\rangle\langle 1| + \frac{\hbar\Omega_2}{2}|3\rangle\langle 2|\right)\exp(-i\omega t) + h.c \tag{2.17}$$

As mentioned before gray molasses cooling based on the exciting of dark state and bright state. As an example the state $|F = 2, m_F = 2\rangle$ of ^{39}K D1 transition is a dark state in the polarization σ^+ and the state $|F = 2, m_F = -2\rangle$ is a bright state in same polarization (Fig.3.3). However when Raman condition of two photon resonance (Raman resonance) is fulfilled $\delta = 0$, $\delta_1 = \delta_2$, additional dark states $|\psi_D\rangle$ and orthogonal bright states $|\psi_B\rangle$

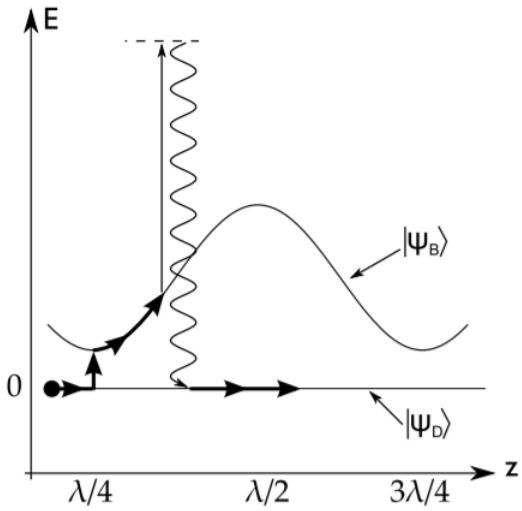

Figure 2.7: Schematic of gray molasses cooling mechanism on three level atom in gradient polarization field with blue detuned light. The ground states splits into bright state $|\psi_B\rangle$ and dark state $|\psi_D\rangle$. The energy of the bright state is positively shifted and spatially modulated. In analogy to Sisyphus cooling, atom moving along the z-axis converts its kinetic energy into potential energy as it climbs the potential hill of the bright state and it looses energy by being pumped back to the dark state via spontaneous emission. The probability for atom to be coupled again to the bright state is inversely proportional to the energy light shift and proportional to the atom velocity. So strong coupling happens at the potential minimum of the bright state and at high atom velocity.[14]

appear, which are coherent superposition of the sublevel states and eigenstates of the Hamiltonian [30]:

$$|\psi_D\rangle = \frac{1}{\sqrt{\Omega_1^2 + \Omega_2^2}}(\Omega_2|1\rangle - \Omega_1|2\rangle) \tag{2.18}$$

$$|\psi_B\rangle = \frac{1}{\sqrt{\Omega_1^2 + \Omega_2^2}}(\Omega_1|1\rangle + \Omega_2|2\rangle) \tag{2.19}$$

we can prove that $|\psi_D\rangle$ is dark by applying the coupling Hamiltonian V on this state:

$$\langle 3|V|\psi_D\rangle = 0 \tag{2.20}$$

which means that $|\psi_D\rangle$ is not coupled to the exited state $|3\rangle$. In same way we can find that the bright state is coupled by the light to the exited state:

$$\langle 3|V|\psi_B\rangle = \frac{\hbar}{2}\sqrt{\Omega_1^2 + \Omega_2^2}\exp(-i\omega t) \tag{2.21}$$

The presence of these additional dark states leads to enhancement of the cooling and achieving lower temperature than the conventional gray molasses, that's why we call it

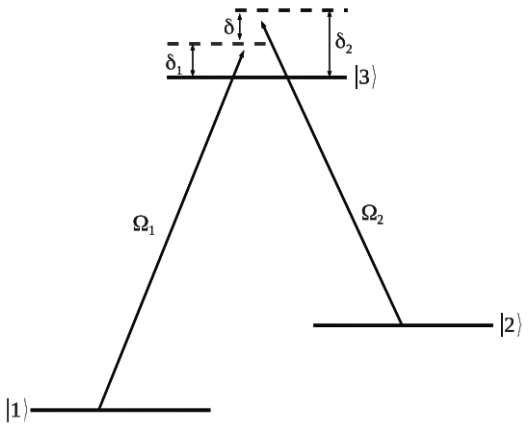

Figure 2.8: Three level Λ-system. Two light fields couple the transitions $|1\rangle \rightarrow |3\rangle$ with detuning δ_1 and $|2\rangle \rightarrow |3\rangle$ with detuning δ_2. The corresponding Rabi frequencies are Ω_1 and Ω_2, respectively [28].

Λ-enhanced gray molasses. For instance the dark state $\frac{1}{\sqrt{2}}(|F = 1, m_F = -1\rangle - |F = 2, m_F = -1\rangle)$ of ^{39}K D1 transition in σ^+ polarization is a coherent superposition of two states $|F = 1, m_F = -1\rangle$ and $|F = 2, m_F = -1\rangle$ with a phase shift of π between them.

Velocity selective coherent population transfer (VSCPT) :
We examine now the coupling probability $\psi_D \rightarrow \psi_B$ as following:
The coupling matrix element between the bright and dark states is [30]:

$$\langle \psi_B | H_{kin} | \psi_D \rangle = -\hbar \frac{2\Omega_1 \Omega_2}{\Omega_1^2 + \Omega_2^2} \frac{kp}{m} \tag{2.22}$$

Where p is the atom momentum and k the wavenumber of transition. From the equation it's obviously to see the dependenc on the velocity $v = p/m$. The Coupling probability $P_{|\psi_D\rangle \rightarrow |\psi_B\rangle}$ can be calculated using the first order perturbation theory [30], which gives:

$$P_{|\psi_D\rangle \rightarrow |\psi_B\rangle} = 2 \left(\frac{\Omega_1 \Omega_2}{\Omega_1^2 + \Omega_2^2} \frac{kp}{\hbar} \right)^2 \delta_1 \left(\frac{\delta_1}{\Omega_1^2 + \Omega_2^2} \right) \tag{2.23}$$

according to this formula the coupling probability is proportional to the square of the atom velocity and inversely proportional to the light shift of the bright state manifested in Rabi frequency. Thus, strong coupling occurs at high velocity and low light shift.

Chapter 3

Gray molasses of Potassium ^{39}K

In this chapter the energy level scheme of ^{39}K is introduced and enhanced sub-Doppler cooling on the D1 transition in gray molasses is explained by presenting all dark and bright states of the atomic system in a polarization gradient field. Finally the advantage of combining the D1 light with the D2 light in the cooling process is highlighted.

3.1 Fine and hyperfine structure of ^{39}K

The fine structure arises from the spin-orbit coupling of the valence electron with the orbital angular momentum **L** and the spin angular momentum **S**. The total angular momentum operator **J** can by expressed as:

$$\mathbf{J} = \mathbf{L} + \mathbf{S}$$

where the quantum number J is in the range of $|L - S| \leq J \leq L + S$
The electronic ground state of ^{39}K is $4^2S_{1/2}$ where L=0 and S=1/2, thus J=1/2. For the first exited state 4^2P, L=1 and S=1/2 which leads to a total quantum number J=1/2 ($4^2P_{1/2}$) and J=3/2 ($4^2P_{3/2}$). Transition to the first sub-level excited state ($4^2S_{1/2} \rightarrow 4^2P_{1/2}$) is called D1 transition and transition to the higher sub-level exited state ($4^2S_{1/2} \rightarrow 4^2P_{3/2}$) is called D2 transition. The corresponding wavelengths are about 770.108 nm and 766.701 nm, respectively.

The hyperfine splitting originates from the interaction between the total angular momentum of electron **J** and the nuclear spin **I**

$$\mathbf{F} = \mathbf{J} + \mathbf{I}$$

the quantum number F is in the range of $|J - I| \leq F \leq J + I$. The nucleus of ^{39}K has a half integer spin I=3/2 due to the odd mass number. In this case the ground state $^2S_{1/2}$,for example, splits into two states separated by 461.7 MHz and associated with the quantum numbers F=1 and F=2 as shown in Fig.3.1. The linewidth $\Gamma/2\pi$ of the D1-line is about 6 MHz (See Tab.3.1 for more details).

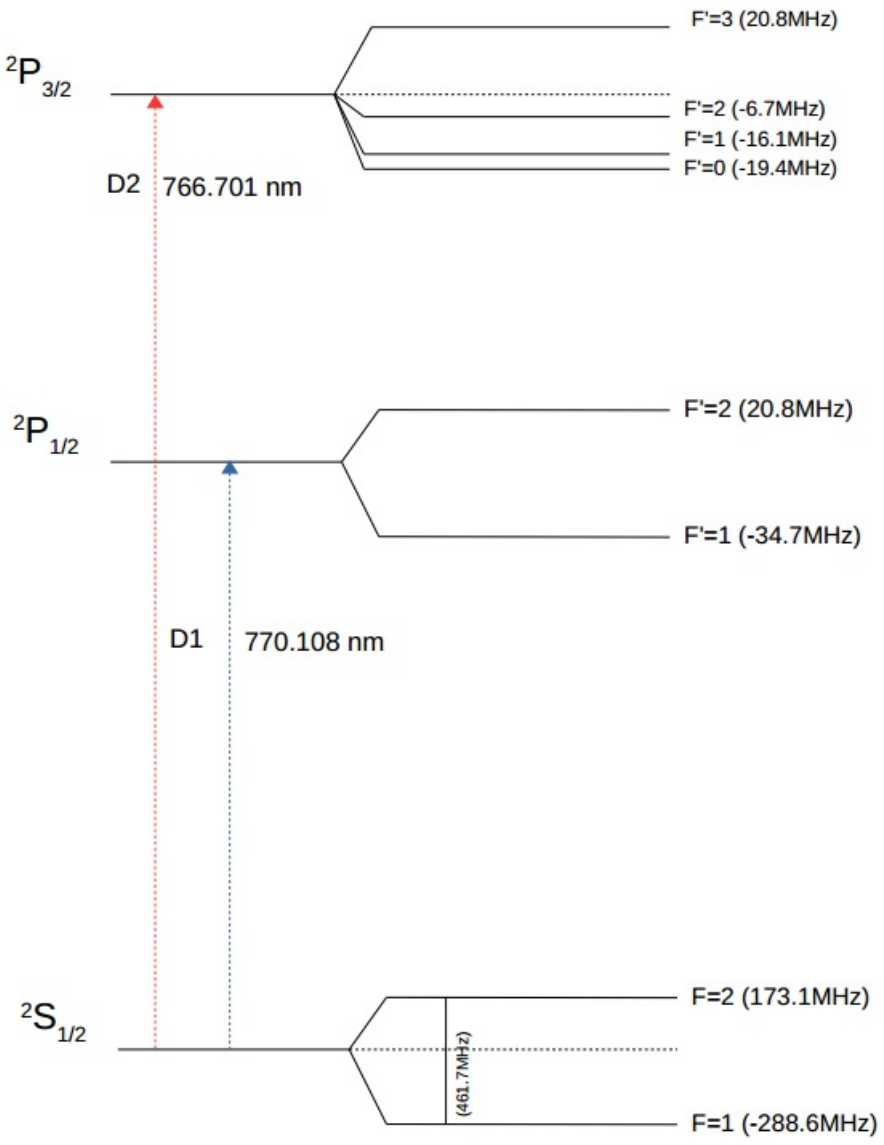

Figure 3.1: ^{39}K level scheme for the ground state $^2S_{1/2}$ and the first two exited states $^2P_{1/2}$, $^2P_{3/2}$ with the hyperfine splitting. [42]

Wavelength	λ	770.108385049(123) nm
Frequency	ν	389.286058716(62) THz
Lifetime	τ	26.72(5) ns
Natural linewidth	$\Gamma/2\pi$	5.956(11) MHz
Doppler Temperature	T_D	145 μK
Recoil Temperature	T_{rec}	0.41436702 μK
Saturation intensity	I_s	1.75 mW/cm^2

Table 3.1: Optical properties of the ^{39}K D1-line [42]

3.2 Enhanced sub-Doppler cooling on the D1 transition of ^{39}K in gray molasses

In analogy to the Λ-configuration, a gray molasses cooling on the D1-line of ^{39}K can be implemented by two light fields detuned above the D1-transition as illustrated in Fig.3.2. The cooling beam has a frequency ω_C corresponding to the transition $|F = 2\rangle \rightarrow |F' = 2\rangle$ plus blue detuning δ_c

$$\omega_C = \omega_{|F=2\rangle \rightarrow |F'=2\rangle} + \delta_c \tag{3.1}$$

and the repumping laser beam has a frequency ω_R corresponding to the transition $|F = 1\rangle \rightarrow |F' = 2\rangle$ plus blue detuning δ_R

$$\omega_R = \omega_{|F=1\rangle \rightarrow |F'=2\rangle} + \delta_R \tag{3.2}$$

The relative detuning is $\delta = \delta_R - \delta_C$. As mentioned before by satisfying Raman condition $\delta = 0, \delta_c = \delta_R$ we can achieve a deep sub-Doppler cooling as extra dark states appear. Table.3.2 presents in this case all possible dark and bright states of the hyperfine structure and the magnetic sublevels of the D1 transition for three different polarization σ^+, π and σ^-. Fig.3.3 shows the D1-transitions in enhanced gray molasses taking to the account the selection rules in Tab.2.1.

3.2.1 Combining the D1 light with the D2 light

As was mentioned in the introduction the aim of this project is not only to achieve lower temperature than that in our current experiment but also to increase the number of trapped potassium atoms and to increase the phase space density. That can be accomplished by using both the D1 light and the D2 light in 3D-MOT followed by a hyper D1-D2 compressed MOT and finally a pure gray molasses cooling using D1 light as reported in [34]. There are two critical parameters for achieving efficient cooling, the detuning and the laser intensity, which have to be set or even ramped during the experiment (See Tab.3.3 for more details).

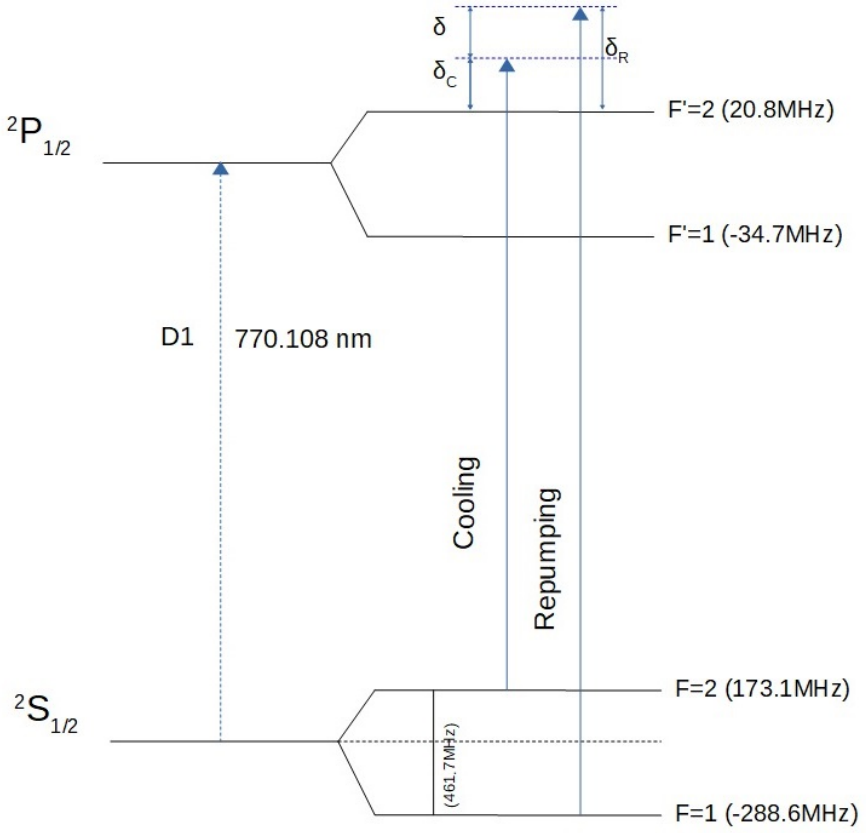

Figure 3.2: Cooling and repumping beams couple the ground states $F = 1$, $F = 2$ to the excited state $F' = 2$ with blue detuning δ_c and δ_R for the cooling and repumping beams respectively. [34]

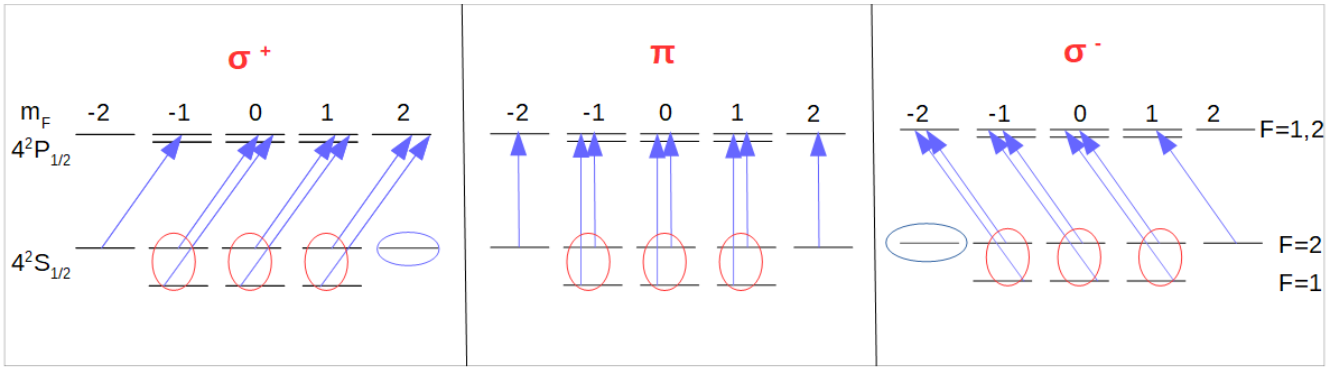

Figure 3.3: The magnetic sublevel states of ^{39}K D1 line with the allowed transitions depending on the polarization in gray molasses. Conventional dark states are marked by blue circles and the additional dark states are marked by red circles.

Pol.	Dark states	Bright states
σ^+	$\|F=2,m_F=2\rangle$	$\|F=2,m_F=-2\rangle$
	$\frac{1}{\sqrt{2}}(\|F=1,m_F=-1\rangle - \|F=2,m_F=-1\rangle)$	$\frac{1}{\sqrt{2}}(\|F=1,m_F=-1\rangle + \|F=2,m_F=-1\rangle)$
	$\frac{1}{\sqrt{2}}(\|F=1,m_F=0\rangle - \|F=2,m_F=0\rangle)$	$\frac{1}{\sqrt{2}}(\|F=1,m_F=0\rangle + \|F=2,m_F=0\rangle)$
	$\frac{1}{\sqrt{2}}(\|F=1,m_F=1\rangle - \|F=2,m_F=1\rangle)$	$\frac{1}{\sqrt{2}}(\|F=1,m_F=1\rangle + \|F=2,m_F=1\rangle)$
π		$\|F=2,m_F=-2\rangle$
		$\|F=2,m_F=2\rangle$
	$\frac{1}{\sqrt{2}}(\|F=1,m_F=-1\rangle - \|F=2,m_F=-1\rangle)$	$\frac{1}{\sqrt{2}}(\|F=1,m_F=-1\rangle + \|F=2,m_F=-1\rangle)$
	$\frac{1}{\sqrt{2}}(\|F=1,m_F=0\rangle - \|F=2,m_F=0\rangle)$	$\frac{1}{\sqrt{2}}(\|F=1,m_F=0\rangle + \|F=2,m_F=0\rangle)$
	$\frac{1}{\sqrt{2}}(\|F=1,m_F=1\rangle - \|F=2,m_F=1\rangle)$	$\frac{1}{\sqrt{2}}(\|F=1,m_F=1\rangle + \|F=2,m_F=1\rangle)$
σ^-	$\|F=2,m_F=-2\rangle$	$\|F=2,m_F=2\rangle$
	$\frac{1}{\sqrt{2}}(\|F=1,m_F=-1\rangle - \|F=2,m_F=-1\rangle)$	$\frac{1}{\sqrt{2}}(\|F=1,m_F=-1\rangle + \|F=2,m_F=-1\rangle)$
	$\frac{1}{\sqrt{2}}(\|F=1,m_F=0\rangle - \|F=2,m_F=0\rangle)$	$\frac{1}{\sqrt{2}}(\|F=1,m_F=0\rangle + \|F=2,m_F=0\rangle)$
	$\frac{1}{\sqrt{2}}(\|F=1,m_F=1\rangle - \|F=2,m_F=1\rangle)$	$\frac{1}{\sqrt{2}}(\|F=1,m_F=1\rangle + \|F=2,m_F=1\rangle)$

Table 3.2: Dark and bright states in the dressed state picture of ^{39}K when Raman condition is satisfied in three pure polarization of light σ^+, π and σ^-.

Stage	D1-Cooling beam	D1-Repumping beam
MOT with D1	$\delta_C = 0$ (resonat light), $I_C = 1.5I_S$	$\delta_R = 0$, $I_R = 0.5I_S$
D1-D2 CMOT	$\delta_C = 3.5\Gamma$, $I_C = 3.5I_S$	No repumping beam
D1 gray molasses	$\delta_C = 3.5\Gamma$, ramping down from $I_C = 3.5I_S$ to $I_C = 0.2I_S$	$\delta_R = 3.5\Gamma$, $I_R = 1.2I_S \rightarrow I_R = 0.07I_S$

Table 3.3: The experimental sequences for cooling potassium atoms using D1+D2 light and pure gray molasses with the optimal values of detuning and intensity per beam according to [34] (the optimal parameters values of the D2 light can be found in the same reference). Note that $\Gamma/2\pi$ is the natural linewidth of the D1 line ($\approx$ 6MHz) and I_S the saturation intensity (1.75mW/cm^2).

From this point of view and in order to realize a D1 laser system we need a laser source with a single frequency close to the D1 transition (389.286058716(62) THz) and in some way there must be a control on this frequency to shift it in the MHz range to generate the cooling and repumping light with a total optical power of several hundred mW [1]

In the next chapter we introduce the design and the construction of our D1 laser system, which consists of three subsystems categorized in:
1- **Frequency locked seed laser system**: it includes the laser source (low power laser diode with a maximum output power less than 100mW) with its locking system for frequency stabilization in the long and short term to on of the atomic transitions of D1-line of ^{39}K.
2- **Tapered amplifier system**: for amplifying the seed power to several hundred mW to obtain the required power for gray molasses cooling if we consider the power loss inside the optical components of the system.
3- **Double pass acousto-optic modulator system**: for shifting the locked laser frequency to the required cooling and repumping frequencies with blue detuning using two acousto optic modulators with central drive frequency of 110MHz.

[1] Considering four horizontal beams and one vertical beam with an average diameter of 2.2 cm per beam in the science chamber and taking into account the saturation intensity I_s of Potassium ^{39}K we calculate the required cooling power considering $I_C = 3.5I_s$ and we calculate the required repumping power considering $I_R = 1.2I_s$. As a result, it would be ≈23.28 mW per beam for the cooling and ≈7.98 mW per beam for the repumping, which gives a total required power of ≈156.3 mW.

Chapter 4

Laser system setup

4.1 Seed Laser

This section introduces the seed laser (master laser) of the system, which is a GaAs semiconductor laser diode with Fabry-Perot cavity and ridge waveguide used in external cavity with interference filter as a frequency selective element. First we take a look on the basics of semiconductor laser diode. Next we explain the principle of mode selection. Finally we present the design and the construction of the seed laser.

4.1.1 Semiconductor Laser diode (LD)

Diode lasers have been widely used in ultracold atoms experiments for many reasons including their high power conversion efficiency upto 50% because they are electrically pumped. In addition they have long lifetime and compact size. Further more they have lasing in the near infrared-range and they are not expansive compared to other types of lasers [5].

Basics of semiconductor diode lasers

Electronic band structure of semiconductor
The energy levels in Gas and solid-state lasers are almost as sharp as those of isolated atoms. However, in semiconductor the discrete energy levels of atom overlap to form electronic bands as illustrated in Fig.4.1. At the absolute zero $T = 0$K and when there is no external excitation all electrons occupy the lower band, which called valence band, while the upper band called conduction band is empty. The probability of occupation can be expressed in terms of Fermi level E_F, which is at $T = 0$ in the middle between the lowest energy level of the conduction band E_c and the highest energy level of the valence band E_v. The two bands are separated by a forbidden energy band called bandgap E_g, which has a value of Eg = 0.5–2.5 eV [9]. Pumping the system with energy (optically, electrically etc.) can cause electron to be exited to the conduction band leaving a hole (missing electron) behind it in the valence band. These both two types of carriers

(electron-hole) can contribute to the conduction. The kinetic energy E of free electron in terms of it's wavenumber k is given by:

$$E(k) = \frac{p^2}{2m_0} = \frac{(\hbar k)^2}{2m_0} = \frac{\hbar^2 k^2}{2m_0} \tag{4.1}$$

in semiconductor the energy of electrons in the conduction band and valence band is also a parabolic function of the wavenumber as shown in Fig.4.2

$$E_c(k) = E_g + \frac{\hbar^2 k^2}{2m_e}, \qquad E_v(k) = -\frac{\hbar^2 k^2}{2m_h} \tag{4.2}$$

where m_e and m_h are the effective mass of electron and hole, respectively.

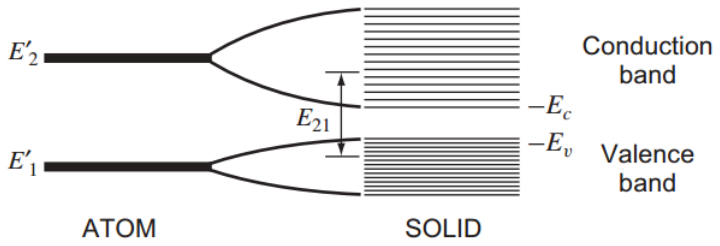

Figure 4.1: Energy bands in semiconductors consist of many levels rather than in atom with decrect energies. [5]

Doping of semiconductor (n-type and p-type)
Adding impurity atoms to an intrinsic semiconductor crystal would improve its conductivity by contributing extra electrons to form n-type semiconductor or generating extra holes (p-type semiconductor). The Fermi level is located close to the conduction band at room temperature for n-type, while it is close to the valence band for p-type.

Generation and recombination
Radiative transition between the valence and conduction bands is always associated with absorbing photon or emitting photon with energy $\hbar\omega = E_2 - E_1$. As shown in Fig.4.3 there are three different types of radiative transitions: absorption, spontaneous emission and stimulated emission. Spontaneous emission occurs when electron in the conduction band recombines with a hole in the valence band emitting photon. This kind of recombination generates incoherent photons like the LED light. The inverse process of recombination is generation of electron-hole pair by absorbing photon. The basic idea of semiconductor laser is to generate a coherent light, which is dominated by stimulated recombination, when the recombination of electron-hole takes place by stimulation from a present photon. consequently, a new photon with the same direction, phase and frequency is emitted. It should be noted that obtaining an optical gain is only possible by stimulated recombination.

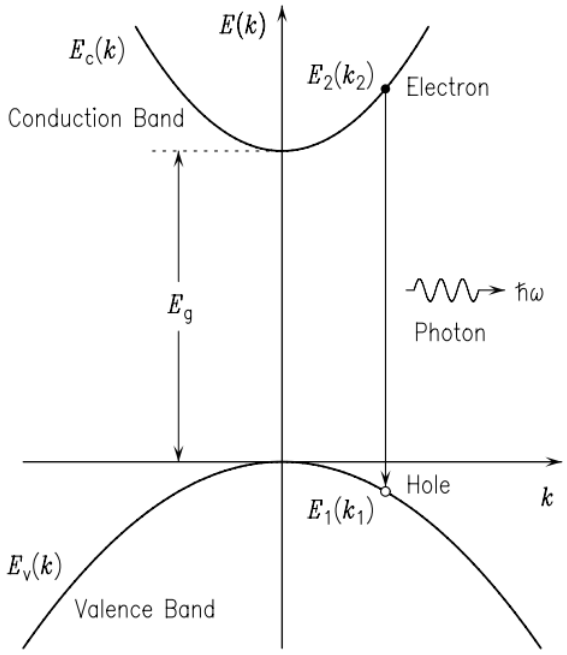

Figure 4.2: Electron energy as a function of the wave vector magnitude $E(k)$ in semiconductor with direct bandgap. [9]

In thermal equilibrium with the radiation field the rate of absorption R_{12} is equal to the rate of radiative recombination (R_{sp} spontaneous emission rate + R_{21} stimulated emission rate):

$$R_{12} = R_{sp} + R_{21} \tag{4.3}$$

this equation can be represented by the spectral photon density $\rho(\hbar\omega)$ and Einstein coefficients, which gives:

$$B_{12} = B_{21} = B, \qquad A_{21} = \frac{n^3}{\pi^2\hbar^3c^3}(\hbar\omega)^2 B \tag{4.4}$$

where A_{21} the transition probability for spontaneous emission, B_{12} the transition probability for absorption and B_{21} the transition probability for stimulated emission.

Double-heterostructure p-i-n junction

In non-equilibrium the Fermi level E_F splits into two different quasi Fermi levels for the conduction and valence bands E_{F_c} and E_{F_v}. In this case the ratio of R_{12} to R_{21} is given by:

$$\frac{R_{12}}{R_{21}} = \exp\left(\frac{\hbar\omega - (E_{F_c} - E_{F_v})}{k_B T}\right) \tag{4.5}$$

One important condition to generate laser light is to achieve optical gain and population inversion of the carriers, meaning when more electrons can be found in the conduction

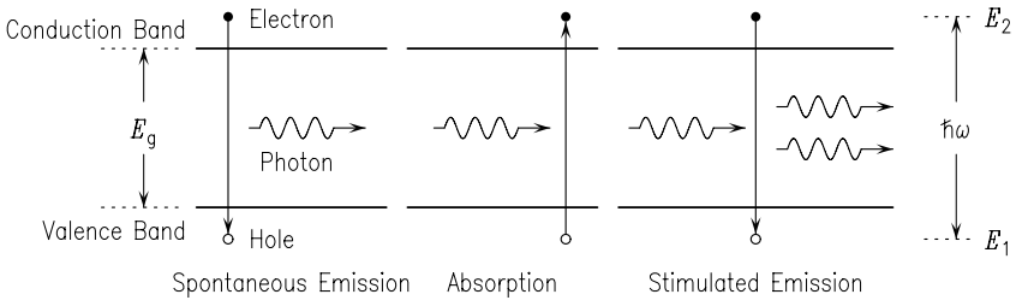

Figure 4.3: Radiative transitions in semiconductor. Right: stimulated emission occurs at presence of a photon with energy $\hbar\omega = E_2 - E_1$. Middle: electron in the valence band is exited to the conduction band by absorbing photon with energy higher than the bandgap E_g. Left: electron from the conduction band recombines spontaneously with a hole in the valence band emitting photon.[9]

band than in the valence band. In other words, when the rate of stimulated emission is greater than the rate of absorption $\frac{R_{12}}{R_{21}} < 1$, that can be satisfied from equation 4.5 when:

$$E_{F_c} - E_{F_v} > \hbar\omega > E_g \tag{4.6}$$

this condition can be realized in the active area of forward biased double-heterostructure diode. An intrinsic semiconductor material with low bandgap is sandwiched by higher bandgap semiconductors n-type and p-type. When applying a forward-bias voltage, carries (electrons and holes) are injected from the n- and p-type areas into the intrinsic layer (active region) where $E_{F_c} - E_{F_v} > E_g$. Consequently, a carrier inversion and light amplification by stimulated emission of radiation are achieved as sketched in Fig.4.4. The active region acts also as a waveguide along it's transverse axis thanks to the low refractive index compared with that for the cladding layers. The waveguide provides a confinement for photons in the intrinsic layer and hence we can obtain the required high photon density $\rho(\hbar\omega)$ to suppress spontaneous emission according to the equation [9]:

$$\frac{R_{sp}}{R_{21}} = \frac{B}{A_{21}}\rho(\hbar\omega) = \frac{\pi^2\hbar^3c^3}{n^3(\hbar\omega)^2}\rho(\hbar\omega) \tag{4.7}$$

and the double-heterostructure confines the charge carriers in the active region.

Fabry-Perot Laser Diodes with ridge waveguide

The most common type of diode lasers is Fabry-Perot laser diode, which has a double-heterostructure and Fabry-Perot cavity formed by the two surfaces of the active region along its optical axis due to the difference in the refractive index between the the surface and the surrounding air. The rear facet is high reflection coated. A narrow waveguide and a small refractive index step between the active region and the cladding layers can improve the laser transverse mode (spatial mode) to be single mode nearly Gaussian with

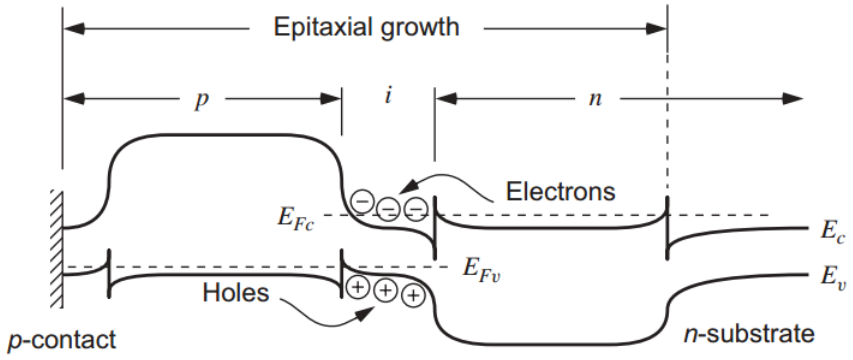

Figure 4.4: Energy band digram of double-heterostructure diode [5]. Full explanation in text.

diffraction-limit. In Ridge waveguide laser diode the index step is obtained by a step in the width of the upper cladding layer (Fig.4.5). The ridge waveguide structure provides current and photon confinement [5].

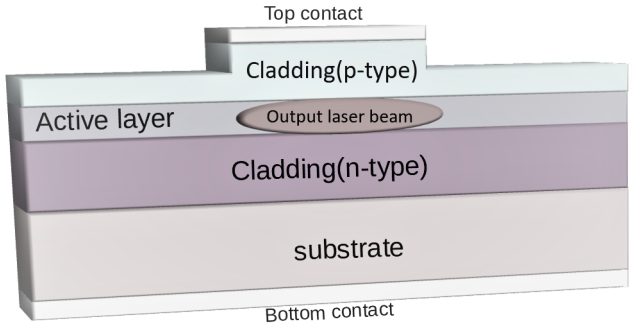

Figure 4.5: Schematic of ridge waveguide laser diode.

Beam profile of laser diode

The cross section of the active layer of a laser diode has a rectangular shape and because of the limited confinement the laser is emitted with elliptical shape. The beam divergence is larger in the vertical direction than in horizontal, therefore the vertical direction is called fast axis and the horizontal is called slow axis. As the laser beam propagates, the beam becomes elliptical in the vertical direction because it's more divergent.
The spherical aberration caused by the large divergance in the vertical axis can be corrected using a collimating lens, which must have at least one aspheric surface and in order to avoid severe beam truncation the numerical aperture NA must be at least 0.3 [39]. The laser beam is also astigmatic because of the rectangular shape of the active

region and the changing in the gain profile across the active layer in the horizontal axis. As shown in Fig.4.6 the location of the beam waist is different in the slow axis than in the fast axis.

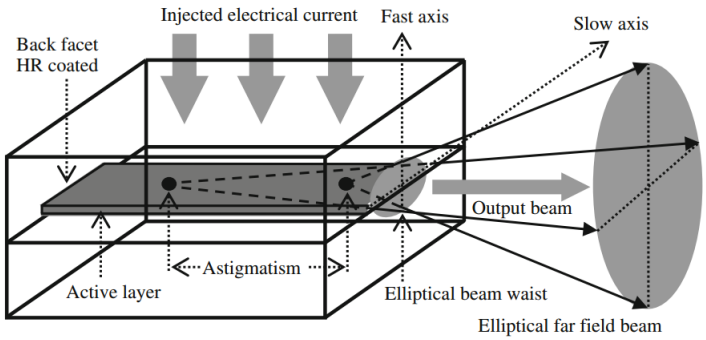

Figure 4.6: elliptical beam profile of a laser diode shows astigmatism, where the focal point of the fast diverging axis lies at the output facet and the focal point of the slow diverging axis located somewhere inside the active layer [39].

Optical spectrum of laser diode

Under threshold current the optical spectrum of laser diode is very broad as shown in Fig.4.7. The laser diode operates above threshold in multiple longitudinal modes with different gain values and high gain at the center wavelength λ_c as illustrated Fig.4.8. The number of modes depends on the length of the Fabry-Perot cavity L and the operation current. The length of the cavity is an integer number m of half wavelengths λ, $L = m\lambda/2$ where $\lambda = \lambda_0/n$, n the refractive index of the waveguide. Modes are spaced by the free spectral range of the resonator $\Delta\lambda = \frac{\lambda_0^2}{2nL}$.

It should be noted that the center Wavelength of a laser diode is shifted linearly when increasing the temperature.

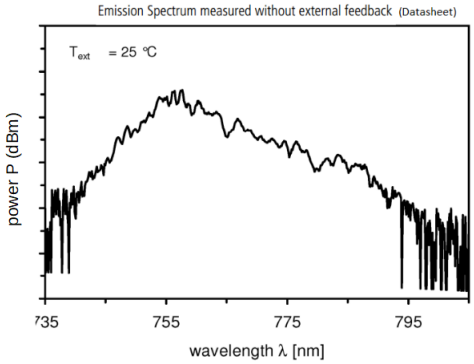

Figure 4.7: Laser diode spectrum below threshold and without feedback from external cavity [13].

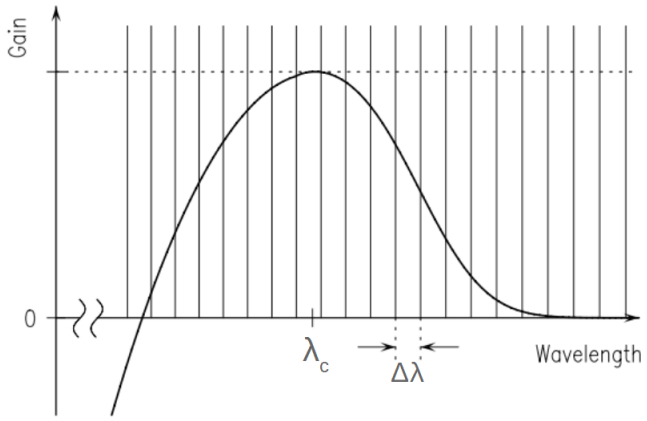

Figure 4.8: Laser diode modes above threshold with the corresponding gain. The gain has its maximum value at the center wavelength λ_c. [9]

Laser diode used for our system
We use a tunable GaAs semiconductor laser diode with a Fabry-Perot cavity and ridge waveguide from eagleyard Photonics (EYP-RWE-0780-02000-1300-SOT12-0000). The tuning range of the laser wavelength is $760 - 790$ nm with base wavelength $\lambda_c = 780$ nm. The maximum allowed current according to the datasheet is 180 mA. The laser diode is in SOT package style, which includes also a monitor photodiode to maintain the output power at constant value Fig.4.9.

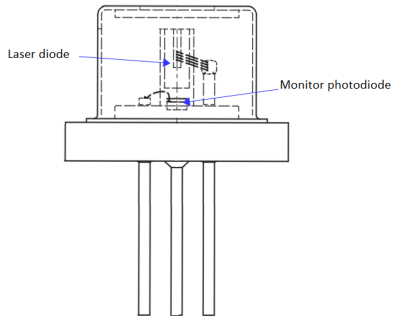

Figure 4.9: Laser diode and monitor photodiode in SOT package style

4.1.2 Interference-filter-stabilized external-cavity diode laser (ECDL)

For a single longitudinal mode operation we couple the laser diode to an external cavity, in which only one mode is selected via wavelength selection element. Many configurations have been implemented for this purpose. For example the Littrow configuration, where the wavelength discriminator is formed by a diffraction grating $\lambda = 2d \sin\theta$ (Bragg condition), where θ is the incident angle and d is the grating's line spacing. However, this arrangement suffers from high sensitivity to misalignment, because the grating acts

as both selective element and out-coupler reflector. Thus, tuning the angle of the grating would influence the optical feed back reflection.
To overcome this problem, the wavelength selection and the feedback have to be separated. This is possible by using an intra-cavity interference filter as frequency selective element and a partially reflective mirror as out-coupler to provide the required feedback reflection. In this way the selection of the wavelength can be done by tuning the angle of the interference filter without affecting the optical feedback.
An interference filter is a Fabry–Pérot etalon, which transmits a certain wavelength λ at a certain angle of incidence θ as the following equation:

$$\lambda = \lambda_0 \sqrt{1 - \frac{sin^2\theta}{n_{eff}^2}} \tag{4.8}$$

where n_{eff} the effective refractive index of the etalon and λ_0 the wavelength at normal incidence.
The external cavity is formed by the highly reflection back facet of the laser diode and the partially reflective mirror mounted on a piezo electric transducer as shown in Fig.4.10. Tuning the voltage applied on the piezo changes the length of the external cavity. Two aspheric lenses are used inside the cavity, one is to collimate the laser diode output beam and the other lens is to focus the laser on the outcoupler mirror, which provides more stability against misalignment [2]. The focusing lens with the mirror are forming cat's eye.

Principle of operation

The length of the internal cavity of the laser diode specified in the datasheet is $L = 1.3$ mm. From the equation $\Delta\nu = c/2nL$ we can calculate the internal modespaceing considering $n = 3.6$ for GaAs, which gives $\Delta\nu_{in} = 32$ GHz, whereas the external modes are spaced by $\Delta\nu_{ex} = 2.6$ GHz assuming $n = 1$ and $L = 57.7$ mm. So the external modes are superimposed on the internal modes, which in turn have different gain values. On the other hand the frequency selective element with it's narrow bandwidth produces a loss to those internal modes outside the bandwidth and a maximum gain at that frequency, which corresponds to the maximum of the interference filter transmission. Consequently we can obtain a stabilized laser with one single internal mode. Fig.4.11 shows the internal and the external modes spectra as well as the interference filter transmission spectrum.

Laser frequency dependence

The laser frequency ν is a function of $f(I, T, \theta, U_{piezo})$, where I, T the laser diode current and temperature, respectively. θ the angle of the interference filter. U_{piezo} the piezo voltage.
Tuning the laser current and the temperature shift the internal modes, while varying the piezo offset changes the external cavity length and hence shifts the external modes. By

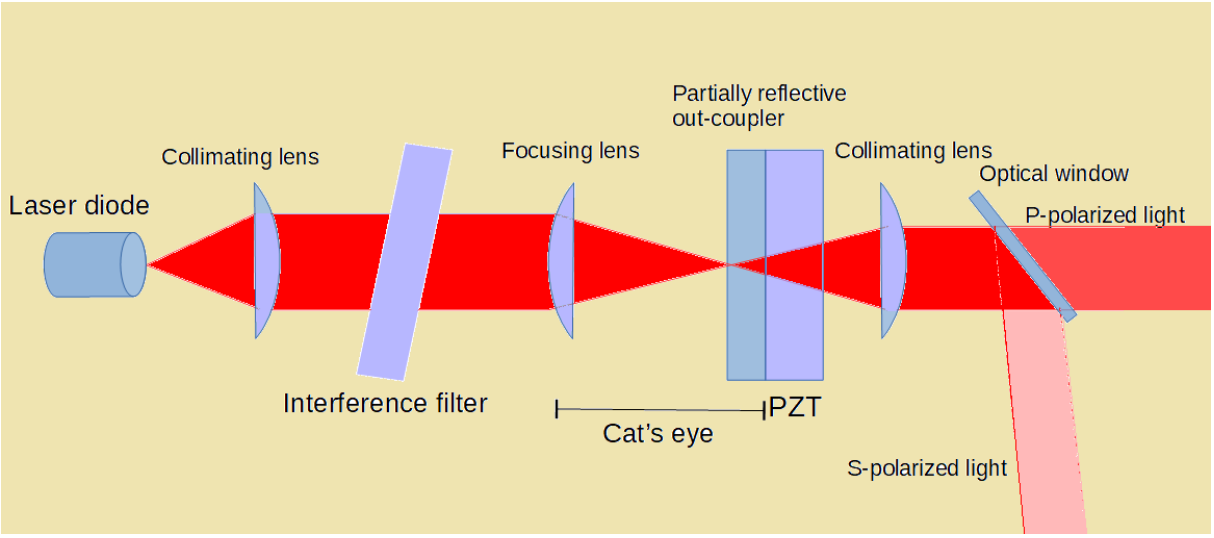

Figure 4.10: Configuration of interference filter stabilized external cavity diode laser. We use an interference filter with nominal wavelength 767nm. The focusing and collimating lenses have focal length f=18.4mm. An out-coupler mirror with 20% reflectivity is glued on a piezo transducer (PZT) from Piezomechanik (HPSt150/14-10/12), which can control the length of the external cavity and an optical window has been mounted at Brewster angle to polarize the output laser beam.

changing the interference filter angle one can shift the transmission maximum and the selected center frequency.

Optical power

Our seed laser has a threshold current of ca.51 mA at $T = 19.6°C$. Above threshold the optical power increases linearly with increasing the current as shown in Fig.4.12. The maximum output power is about 86(4)mW at 180mA (the maximum allowed forward current according to the laser diode datasheet is 180mA). It should be noted that decreasing the temperature leads to increase the optical power.

4.1.3 Beam shaping

As was mentioned before the beam profile of a laser diode has an elliptical shape. It is desirable, however, for a convenient use to convert the beam to a circular symmetric. For this purpose we use an anamorphic lens system (Schäfter+Kirchhoff 5AN-2-V-05 [37]), which consists of positive and negative cylindrical lenses to reduce the beam scale in the long axis to be as that of the short axis as shown in Fig4.13.

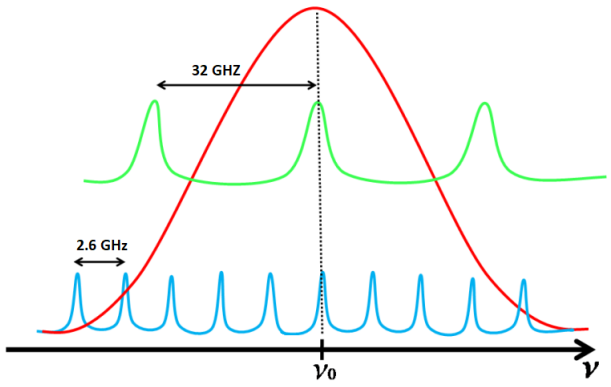

Figure 4.11: Optical modes spectra, internal modes (green), external modes (blue) and the interference filter transmission (red). Adapted from [35]

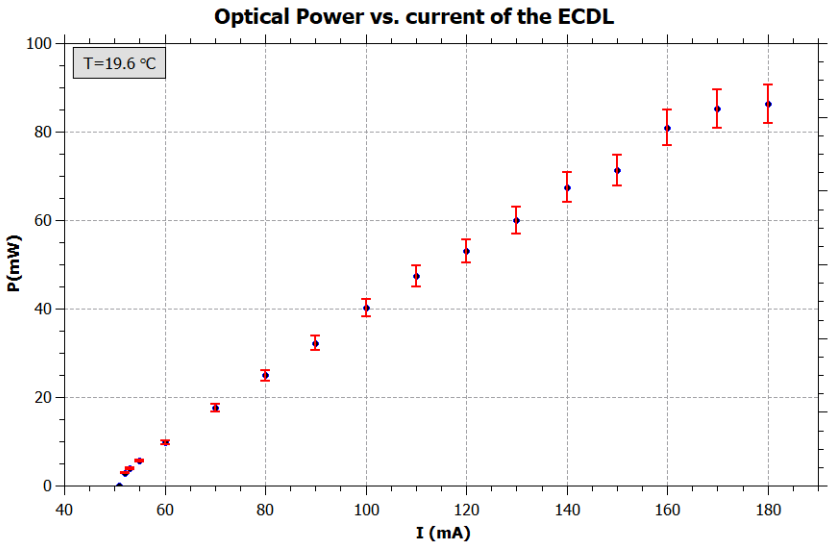

Figure 4.12: ECDL output optical power versus the driving current. The optical power increases linearly above threshold with slop efficiency 0.43(2)mW/mA.

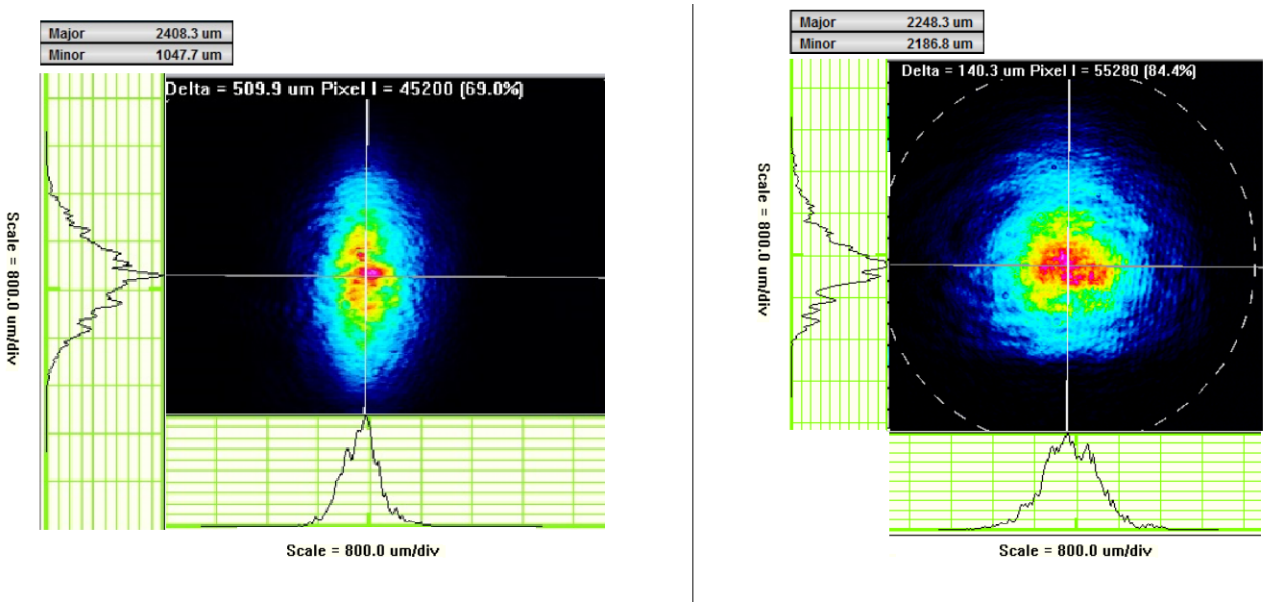

Figure 4.13: ECDL beam profile in the near field with the major and minor diameter in μm unit plus the intensity profile in horizontal and vertical axis recorded by a beam imaging camera and displayed using the software DataRay. Left: elliptical beam profile. Right: nearly circular symmetric beam after shaping (mean diameter is about 2.2mm)

4.2 Laser frequency stabilization

Since we want to perform the laser cooling on the D1 transition of ^{39}K the laser linewidth must be less than the natural linewidth of the D1 transition ($\Gamma/2\pi = 5.956(11)$ MHz). Our free running laser has a linewidth in the kHz range. For more stability and to avoid any frequency drift over time, which can be caused by external noise or temperature fluctuations, we lock the laser frequency to one of the atomic features of the ^{39}K D1-line. First of all we use a technique called saturated absorption spectroscopy in a vapor cell of ^{39}K to resolve its hyperfine structure. Then we lock the laser frequency to a setpoint by generating an error signal using frequency modulation spectroscopy and sending this error signal to a PID controller, which controls the piezo voltage of the ECDL.

4.2.1 Saturated absorption spectroscopy

Doppler broadening

Considering a laser beam propagating in the +z direction through a vapour cell of potassium. When the laser frequency at resonance with an atomic transition ν_0, only atoms with no velocity component along the laser axis can see the laser resonant and consequently absorbing the light, while the laser frequency is Doppler shifted for atoms with velocity component in the z-axis v_z. By tuning the laser frequency to:

$$\nu = \nu_0 \left(1 + \frac{v_z}{c}\right) \tag{4.9}$$

the laser frequency becomes resonant for those atoms with velocity v_z
In thermal equilibrium, v_z has a Maxwell–Boltzmann distribution (thermal distribution):

$$\exp(-mv_z^2/2k_BT) \tag{4.10}$$

from the first equation we can write $v_z = (\frac{\nu-\nu_0}{\nu})c$ and by substituting in 4.10 we find the relative number of atoms at resonance with laser frequency tuned around ν_0, which has a Gaussian lineshape [32]

$$\exp(-mc^2(\nu - \nu_0)^2/2k_BT\nu_0^2) \tag{4.11}$$

as illustrated in Fig.4.14 where the vertical axis taken as the absorption coefficient.
The Full width at half maximum (FWHM) of the Gaussian profile is given by [32] :

$$\Delta\nu = \sqrt{8k_B \ln 2}\ \frac{\nu}{c}\sqrt{\frac{T}{M}} \tag{4.12}$$

From the equation we can calculate the Doppler linewidth of the ^{39}K D1-line at room temperature by setting $\nu_{D1} = 389.2861 \times 10^{12}$Hz, $M = 39 \times 1.67 \times 10^{-27}$Kg, $T = 300$ K, which gives: $\Delta\nu_{D1} \approx 771.5$ MHz. So because of this broad linewidth the conventional absorption spectroscopy can't resolve the hyperfine spectral lines of the D1-transition,

which are closed to each other and have wavelengths around 770 nm. In order to eliminate Doppler broadening and resolve the hyperfine spectral lines we use a method called saturated absorption spectroscopy, which includes two laser beams rather than a single beam.

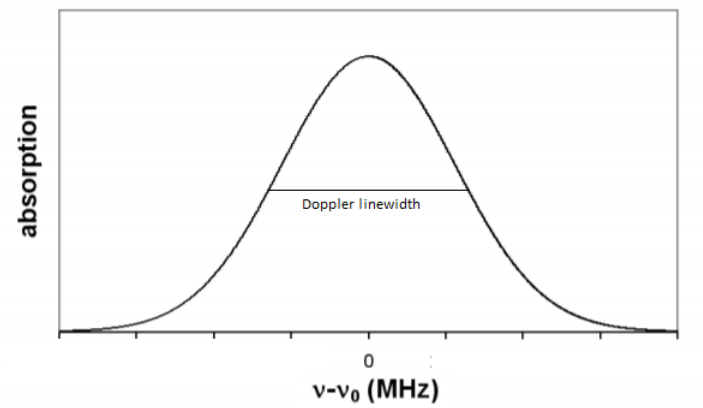

Figure 4.14: The absorption coeffient as a Gaussian function of the laser frequency detuning from resonance. Taken from [23]

Doppler-free saturated absorption

Fig.4.15 shows a typical arrangement of saturated absorption spectroscopy. Two counter-propagating laser beams with the same frequency travel through a sample of an atomic gas and overlap. The laser beam propagating to the left (-z direction) is the pump beam and the retroreflected one is the probe beam, whose absorption is detected by a photodiode.

Two level atom

Assuming a two level atomic gas in a vapor cell with the ground state $|g\rangle$ and exited state $|e\rangle$. The corresponding transition frequency is ν_0. When the laser frequency ν is non-resonant $\nu \neq \nu_0$ the pump and probe beams interact with different groups of atoms. However, when the laser frequency $\nu < \nu_0$ a group of atoms with velocity $-v_z$ interact only with the probe beam as its frequency is blue shifted to ν_0 and they will be exited from the ground state $|g\rangle$ to the exited state $|e\rangle$ (the frequency of the pump beam is for this group of atoms red shifted and not resonant), while other group with velocity $+v_z$ interact only with the pump beam. The number of atoms in the ground state N_g versus the velocity v_z is plotted in Fig.4.16.a. The pump beam is burning a hole (dip) in the ground state population for those atoms, whose velocities in the opposite direction and the probe beam leaves another dip in the same way. As the laser frequency is increasing the two dips become closer and closer. Once the frequency reaches the resonance frequency $\nu = \nu_0$, the pump and probe beams start to interact with same

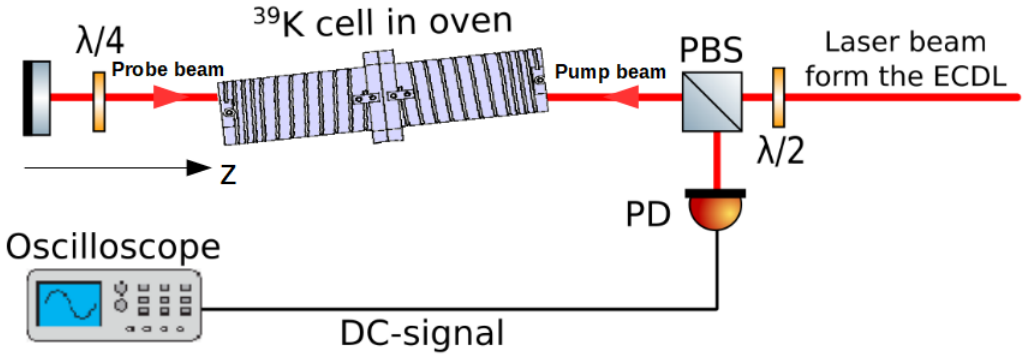

Figure 4.15: The experimental arrangement of saturated absorption spectroscopy. The half wave plate is for tuning the pump beam power and the quarter wave plate is to control the optical power of the beam detected by the photodiode.

group of atoms, which don't have any velocity component in the z-axis. In this case the pump beam causes the exited state to be saturated and the probe beam will transmit with reduced absorption, which leads to a saturated dip as shown in Fig.4.16.b.

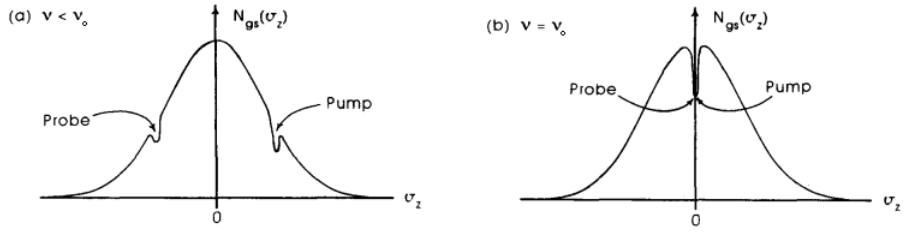

Figure 4.16: The poulation of the gournd state N_{ge} as as a function of atom velocity in one axis v_z. (a) Hole burning is caused by the pump and probe beams when the laser frequency is detuned below the atomic resonance $\nu < \nu_0$. (b) A saturated hole appears at resonance $\nu = \nu_0$.[32]

Three level atom

In case three level system with two resonance frequencies ν_1, ν_2 such as Λ-system (common exited state $|e\rangle$ and two ground states $|g_1>$, $|g_2>$) or V-system (common ground state $|g>$ and two exited states $|e_1\rangle$, $|e_2\rangle$), at a certain frequency ν_c the pump and the probe beams can interact with two groups of atoms at the same time. So the pump beam can excite atoms moving in the same direction as its frequency red shifted to ν_1 and simultaneously atoms moving in the opposite direction as a blue detuned frequency to the ν_2. In both cases one transition can be saturated causing additional dip in the absorption spectrum as depicted in Fig.4.17. Such a frequency is called crossover ν_c,

which can be expressed in terms of ν_1 and ν_2 using equation 4.9 as following:

$$\left.\begin{aligned}\nu_1 &= \nu_c\left(1-\frac{v_z}{c}\right)\\ \nu_2 &= \nu_c\left(1+\frac{v_z}{c}\right)\end{aligned}\right\} \qquad \Rightarrow \nu_c = \frac{\nu_1+\nu_2}{2} \tag{4.13}$$

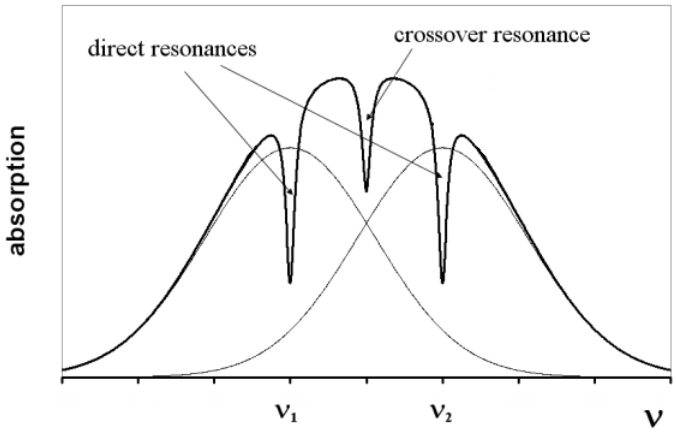

Figure 4.17: Doppler free absorption singal for three level atom. A crossover dip appears at frequency in the middle between ν_1 and ν_2. Adapted from [23]

Saturated absorption spectroscopy of the D1 line of potassium ^{39}K
The Doppler free absorption spectrum of the ^{39}K D1-line shows four direct resonance frequencies ($\nu_{11}, \nu_{12}, \nu_{21}, \nu_{22}$, where: ν_{ge}, g denotes the ground state and e denotes the exited state) and five crossover frequencies, as illustrated in Fig.4.18, divided in three categories:
1- Crossover frequencies resulting from direct transitions in Λ-configuration:

$$\nu_{c1} = \frac{\nu_{11}+\nu_{21}}{2} \tag{4.14}$$

$$\nu_{c2} = \frac{\nu_{12}+\nu_{22}}{2} \tag{4.15}$$

2- Crossover frequencies resulting from direct transitions in V-type:

$$\nu_{c3} = \frac{\nu_{12}+\nu_{11}}{2} \tag{4.16}$$

$$\nu_{c4} = \frac{\nu_{22}+\nu_{21}}{2} \tag{4.17}$$

3- Crossover frequency resulting from direct transitions in a configuration without common ground or exited states:

$$\nu_{c5} = \frac{\nu_{12} + \nu_{21}}{2} = \frac{\nu_{11} + \nu_{22}}{2} \tag{4.18}$$

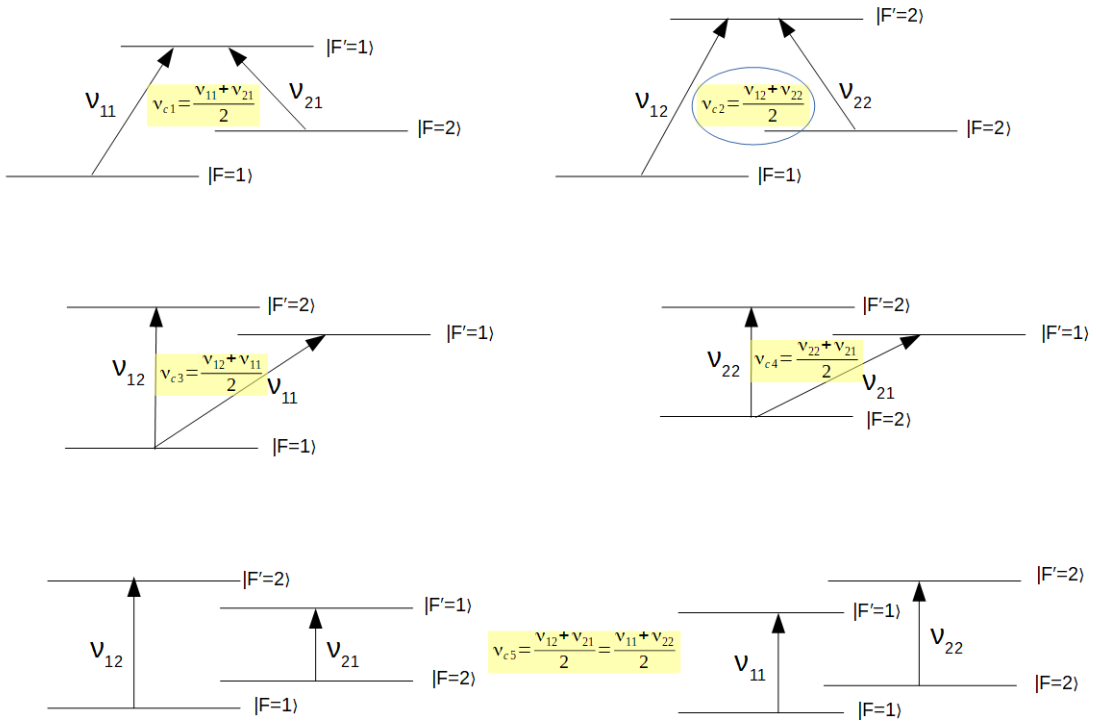

Figure 4.18: Possible transitions between the hyperfine levels of the ^{39}K D1-line in different configurations with the corresponding crossover frequencies in saturated absorption spectroscopy.

Before getting started with the experimental spectroscopy one should note that the vaopr inside the Potassium reference cell, shown in Fig.4.19, has a low pressure $p = 1.3 \times 10^{-8}$ mbar at room temperature $T = 293$ K[42], so we need a heater to increase the vapor pressure and consequently obtain a strong absorption signal. The heating element is an isolated resistance wire (Conrad 429909-62) coiled around an aluminium cylinder. The coiling is done in the clockwise and counterclockwise direction to avoid any magnetic hyperfine splitting of Potassium atoms. To maintain the heater temperature we use a DC regulated power supply. The cell is heated up to $69.4°C$ by a current of 0.48A at a voltage 9.3V.
We scan the laser frequency by varying the piezo offset. The saturated absorption signal is then recorded by a photodetector and displayed on an oscilloscope as shown in Fig.4.20.

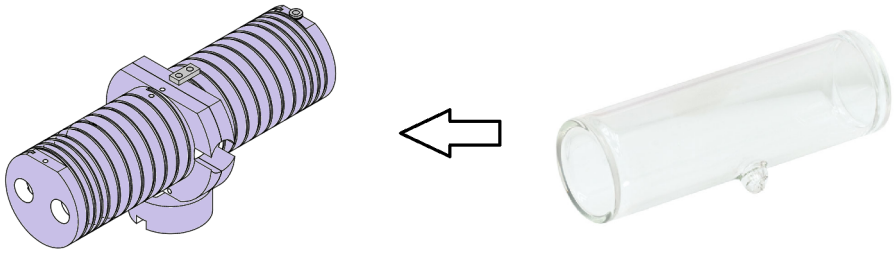

Figure 4.19: Right: Potassium borosilicate reference cell, Ø25 mm x 71.8 mm (GC25075-K) [41]. Left: drawing of the oven

4.2.2 Locking the laser frequency

After we have the absorption signal we want to lock the seed laser frequency to one of the absorption features of the D1-line. We use the so-called frequency modulation spectroscopy to generate an error signal, which is fed back to the piezoelectric transducer of the ECDL via proportional-integral-derivative (PID) controller. We explain next the principle of the FM spectroscopy to present then our locked seed laser system.

Frequency modulation (FM) spectroscopy

Consider we modulate the current of the ECDL by a sine wave generator with a modulation frequency ω_m and modulation amplitude I_m:

$$i(t) = I_0 + I_m \sin(\omega_m t) \tag{4.19}$$

where I_0 is the DC component.
As was mentioned before the frequency of a diode laser depends on the current due to its effect on the refractive index of the active medium and the cavity length [25]. Besides, the optical output power is a function of the current. As a consequence the frequency and the amplitude of the laser radiation is modulated, so we can write the electric field of the laser light as:

$$E(t) = E_0 \exp[i(\omega_0 t + M \sin \omega_m t)] \tag{4.20}$$

where E_0, ω_0 the electric wave amplitude and frequency, respectively and M the modulation index. The equation can be represented in terms of Fourier series expansion:

$$E(t) = E_0 \exp(i\omega_0 t) \sum_{n=-\infty}^{n=+\infty} J_n(M) \exp(in\omega_m t) \tag{4.21}$$

which means that the modulated light has n-frequency components at sidebands spaced by $n\omega_m \pm \omega_0$ with amplitudes defined by Bessel functions $J_n(M)$ of the nth order and argument M, where n is an integer number. Because of the symmetry property $J_{-n}(M) = (-1)^n J_n(M)$, the even and odd order sidebands are in and out of phase, respectively.

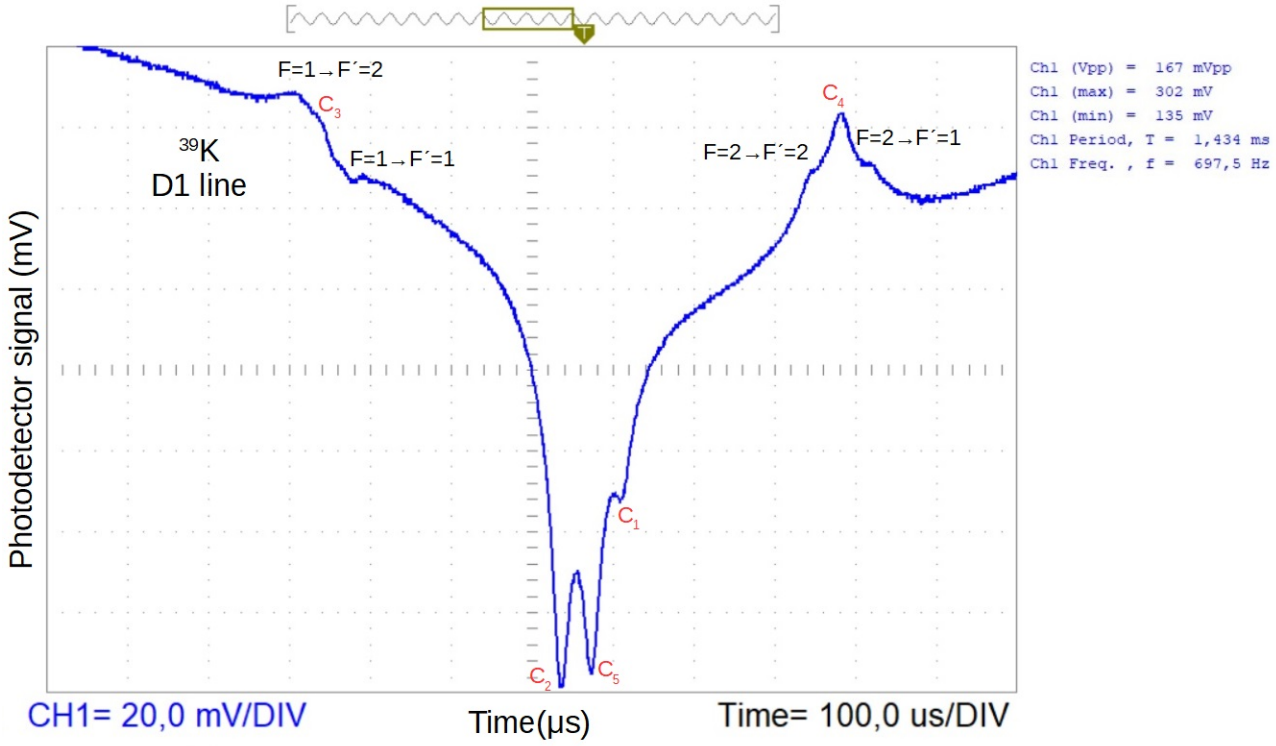

Figure 4.20: Doppler free absorption signal of the D1 line of ^{39}K displayed on an oscilloscope, while scanning the cavity of the ECDL. Taken at a cell temperature 69.4°C and a pump power of 3mW. The hyperfine features and the crossover peaks $(c_1, c_2, c_3, c_4, c_5)$ are labelled. As we will see later we lock the laser to that frequency which corresponds to the deepest peak crossover c_2.

Consequently, the amplitude modulation resulted from two symmetric sidebands are out of phase and exactly cancel out leaving pure frequency modulation [38].
Now let's assume the laser beam is propagating through a probe of a length L with refractive index $\eta(\omega)$ and absorption coefficient $\alpha(\omega)$. We can define also the phase shift ϕ and the attenuation δ for each component as [20]:

$$\delta(\omega) = \alpha(\omega)L/2 \tag{4.22}$$

$$\phi(\omega) = \eta(\omega)L(\omega_0 + n\omega_m)/c \tag{4.23}$$

note that $\delta(\omega)$ has an absorption profile, whereas $\phi(\omega)$ has a dispersion profile. The transmission function $T(\omega)$ is expressed in terms of δ and ϕ:

$$T(\omega) = \exp(-\delta - i\phi) \tag{4.24}$$

then the transmission electric field through the sample can be written as:

$$E_T(t) = E_0 \exp(i\omega_0 t) \sum_{n=-\infty}^{n=+\infty} T(\omega_n) J_n(M) \exp(in\omega_m t) \tag{4.25}$$

As we see, the transmitted wave is now modulated in the amplitude manifested by the attenuation.
Detecting the transmitted light by a fast photodetector generates a photocurrent that is proportional to the slowly varying intensity envelope $\mid \overline{E_T}(t) \mid^2$. Mixing the detected signal with the modulation signal gives a signal with intensity I_{FM} that depends on the phase difference θ between the rf modulation signal and the saturation signal. The mixer output contains components at DC and integer multiples of ω_m. By attenuating high frequency components using a low-pass filter, under weak modulation condition $M << 1$ when only the first sidebands contribute to the signal $J_0 \approx 1,\ J_{\pm 1} \approx \pm M/2$, we can obtain the error signal:

$$I_{FM} = \frac{cE_0^2}{8\pi} \exp(-2\delta_0)[M(\delta_{-1} - \delta_1)\cos\theta + M(\phi_{-1} + \phi_1 - 2\phi_0)\sin\theta] \tag{4.26}$$

The coefficient of $\cos\theta$ is proportional to the absorption signal, whereas the the coefficient of $\sin\theta$ is proportional to the dispersion, which can be ususaly neglected. If the modulation frequency is low compared with natural linewidth then the in-phase component approaches the derivative of δ [20]. From the equation 4.26 one can notice that in order to achieve a strong signal the phase difference θ has to be matched or the modulation index M has to be increased. Optimizing the absorption can also lead to a strong error signal.

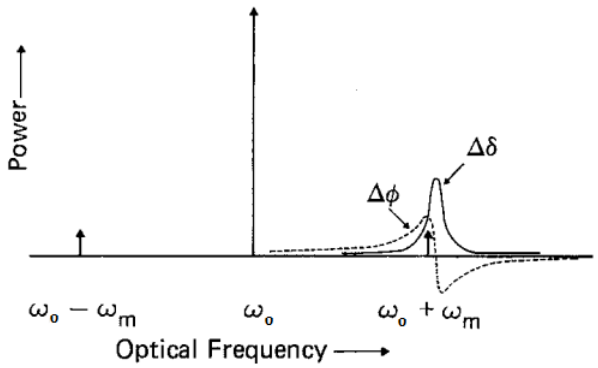

Figure 4.21: Power spectrum in frequency modulation spectroscopy shows the carrier frequency and the first order sidebands when the spectral feature has a Lorentzian lineshap. $\Delta\phi = \phi_1 - \phi_{-1}$ represents the desperation, and $\Delta\delta = \delta_1 - \delta_{-1}$ represents the absorption [3]

Fig.4.22 shows our experimental setup for locking the seed laser. The current of the ECDL is directly modulated with modulation frequency at 400 KHz. Consequently the laser frequency is modulated. The light is then passing through the potassium reference cell as the conventional saturated absorption spectroscopy. The probe beam is detected by a photodiode and the AC-component of the detected signal is multiplied by the modulation signal in a mixer. Only low frequencies are then passing through a low pass filter

with cut-off frequency of 100 KHz and an error signal is finally obtained, which is sent to a proportional–integral–derivative (PID) controller. As mentioned before the error signal is proportional to the derivative of Doppler-free spectrum. thus, the deepest peak in the absorption spectrum of ^{39}K D1-line will correspond to a zero-crossing at the crossover frequency ν_{c2} in the error signal. The zero-crossing frequency acts as a setpoint and the PID controller provides a feedback loop to the seed laser by adjusting the piezo offset to match that frequency with zero-crossing in the error signal. We have record the locked laser frequency with a wavelength meter (the measurement resolution 100 MHz) and we didn't report any frequency drift over 12 hours.

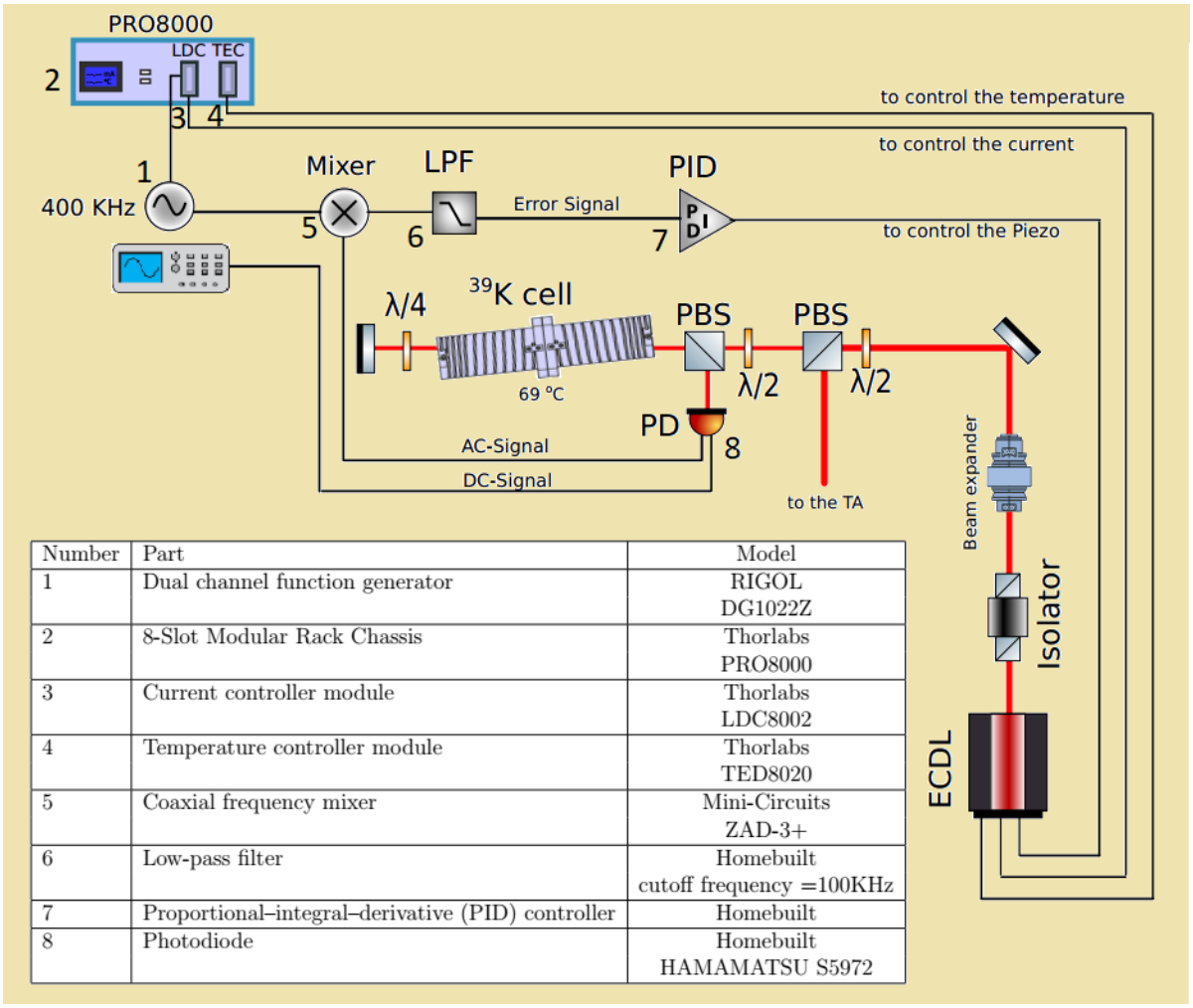

Number	Part	Model
1	Dual channel function generator	RIGOL DG1022Z
2	8-Slot Modular Rack Chassis	Thorlabs PRO8000
3	Current controller module	Thorlabs LDC8002
4	Temperature controller module	Thorlabs TED8020
5	Coaxial frequency mixer	Mini-Circuits ZAD-3+
6	Low-pass filter	Homebuilt cutoff frequency =100KHz
7	Proportional–integral–derivative (PID) controller	Homebuilt
8	Photodiode	Homebuilt HAMAMATSU S5972

Figure 4.22: Setup of the locked seed laser system with a short description of the electronic components and devices used to control the system.

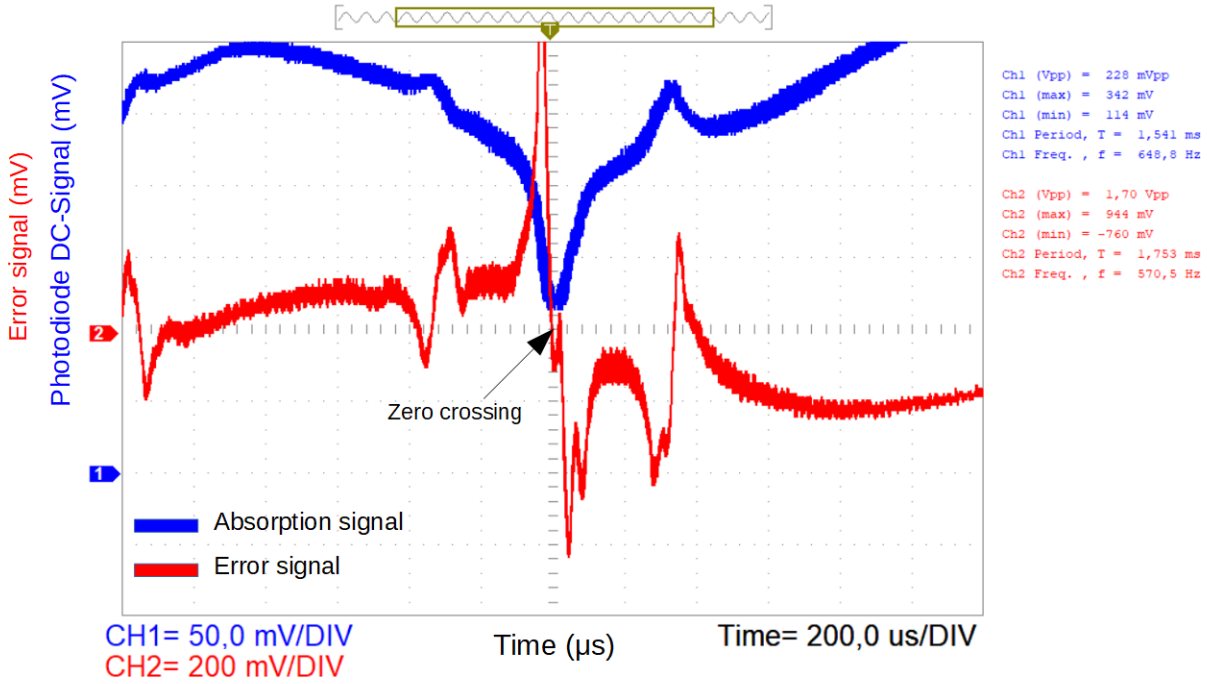

Figure 4.23: FM spectroscopy of Potassium displayed on an oscilloscope. The blue line represents the saturated absorption signal, which is a little bit thick due to the low modulation frequency 400KHz of the injection current. The corresponding error signal (red line) has a zero crossing at crossover frequency $\nu_{c2} = (\nu_{12} + \nu_{22})/2$. We choose this to be as a setpoint for the servo system to stabilize our seed laser frequency.

4.3 Optical power amplification

In this section we present our tapered amplifier (TA) system, which amplifies the seed power from the mW-range to nearly diffraction limited power in the W-range. First we explain the structure of the TA-chip, next we introduce the design of the system including the focusing, the collimating lenses, protecting housing and the control devices. Then we study the TA-output dependence on different parameters related to the seed laser and the TA-current. Finally we show how to improve the beam quality of the TA.

4.3.1 Tapered amplifier (TA)

Structure of a tapered amplifier chip

A tapered amplifier is laser diode with a gain region and electrically pumped tapered contact. The input beam grows as it propagates from the small rear facet to the large front facet. Both facets are anti-reflection coated of less than 0.01%. The length of the tapered region is typically 2 mm. The typical width of the output aperture at front side is 200 μm (for our TA is 256 μm), while it's only 5-10 μm for the input aperture width. The full angle of the taper is usually about 6° [44]. The advantage of such structure is to make a divergent beam and consequently achieve stability to avoid non-linear optical effects such as filamentation or self focusing of the beam. The epitaxial layer structure of the TA is designed as following (Fig 4.24):
1- on the top is a tapered contact layer, which is electrically pumped.
2- in the middle is the active layer (InGaAs), which is optically pumped. It forms a quantum-well region and surrounded by waveguide layers, whose refractive index higher than the clad layers.
3- on the bottom is the substrate.
Cavity spoiling grooves are etched through the gain region to diffract unwanted modes away from the tapered gain region [44].
Now consider an input Gaussian beam focused onto the small input aperture of a TA propagating through the active area. The optical gain increases slowly in the edge before saturation, whereas the gain in the center of the beam increases faster because of the high intensity. At the end the output beam will have nearly homogeneous distribution, so that the beam profile is top-hat and not Gaussian anymore.

Amplified spontaneous emission (ASE)

A TA can also work without optical injection by amplified spontaneous emission (ASE) having a very broad spectrum as illustrated in Fig.4.25 (the blue line). The total output power of a seeded TA contains two fractions. One fraction is ASE and the other is amplified seed signal. The spectrum in this case is represented by the red line in Fig.4.25. The contribution of ASE to the total output power can be reduced by increasing the seed power. However, the TA can be satureted at high seed power [18]. The ASE suppression

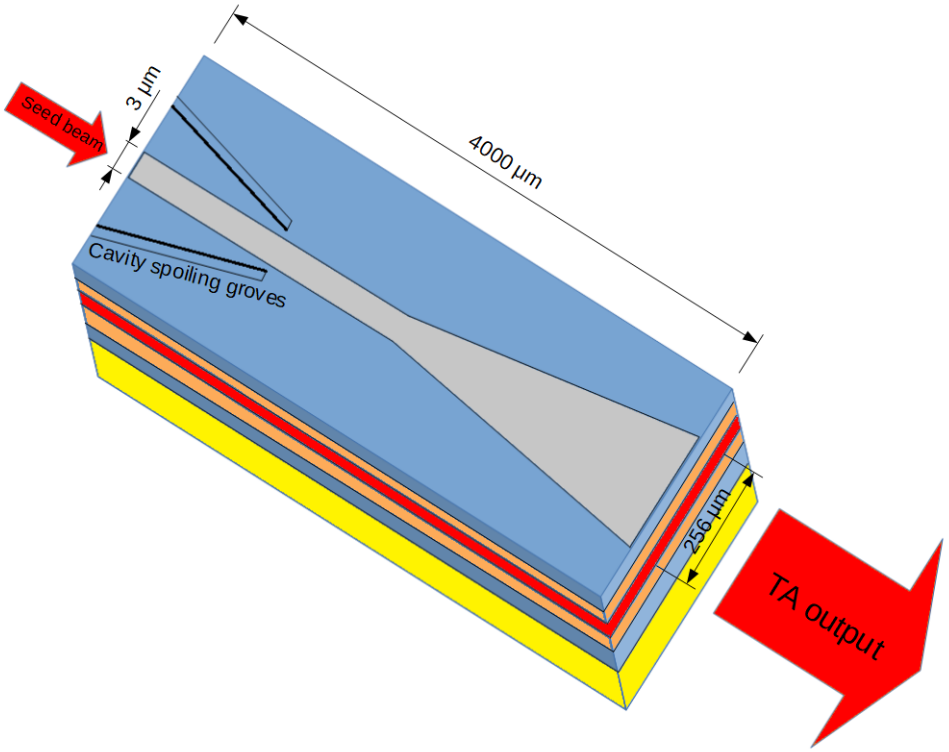

Figure 4.24: Schematic of a tapered amplifier chip. The tapered contact (gray), cladding layer (blue), waveguide (orange), active area (red) and the substrate (yellow). The dimensions belong to our TA chip except the width of the input facet, which is not stated in the data sheet.

of our TA is > 40 dB [10]. the ASE emitted from the rear input can be used for alignment when coupling the seed beam into the TA-chip [21].

4.3.2 Design and construction of the TA system

We use a TA chip in C-mount packaging. The maximum output power is 2 W and the central wavelength is 765 nm. The chip is mounted on a copper holder and a thermoelectric cooler (TEC) is used to regulate the TA temperature. The heat sink is made of Aluminium. A plexiglas housing is used for protecting the TA-chip against dust, which can be burned onto the facets of the chip [21]. The design of the TA system is illustrated in Fig.4.26.
An aspherical lens with focal length f=4.51 is used to focus the seed beam onto the small input facet of the TA chip. The output beam of the TA is asymmetric, astigmatic and strongly divergent, that's why we use a combination of two lenses to collimate the beam in two orthogonal direction. An aspherical lens with focal length f=4.51 collimates the output beam in the vertical direction and a plano-convex cylindrical lens (f=50) collimates the TA-beam in the horizontal direction as shown in Fig4.27. XYZ translation

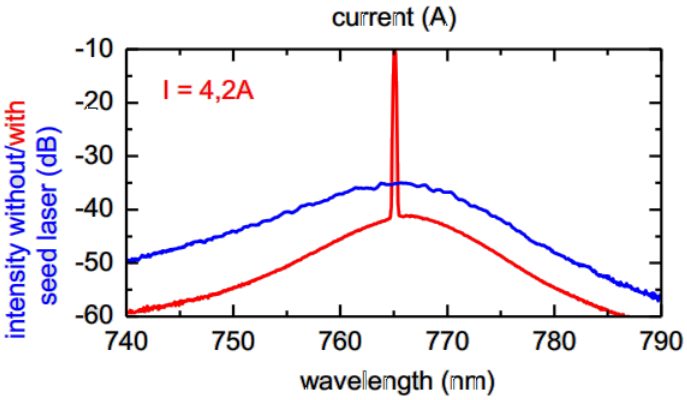

Figure 4.25: Intensity distribution of our TA output versus wavelength in two cases: without optical injection when only amplified spontaneous emission contributes (blue spectrum) and with optical injection (red spectrum). High peak intensity at that wavelength of the seed laser (765 nm) appeares and ASE is suppressed [10].

stage has been used to adjust the focusing and the collimating aspherical lenses before being glued and fixed. It has to be mentioned that the distance between the aspheric lens and the cylindrical lens is critical for collimation. We have found the best position of the cylindrical lens to be 70mm away from the aspheric lens.

4.3.3 Current and temperature control

A current driver module LDC8080 from Thorlabs with maximum current of 8A is used to supply the TA chip with electrical power via protection circuit. Note that the wire flag of the TA package has to be cathode and the base plate has to be connected to the anode. One should be careful not to exceed 2A if the TA is not optically injected and 4.5A when the TA is seeded. The TA temperature is monitored by a thermistor sensor (NTC 10k). A thermoelectric cooler (Peltier element) is then used to stabilize the temperature of the TA to a setpoint, which can be set manually on a temperature controller (see Fig.4.28). The recommended temperature from the provider is 20°C.

4.3.4 TA-output power dependence

The optical power of the TA depends on three tunable parameters $P_{TA} = f(I, P_{seed}, Pol.)$ where: I the operation current, P_{seed} the seed power and Pol. is the seed polarization. Fig.4.29 shows the output power as a function of the seed polarization for different angle of polarization at constant current and seed power of 2A and 30mW, respectively. The zero degree corresponds to TM polarization and hence maximum output power. It is remarkable to note from Fig.4.31 that increasing the seed power upto 30mW leads to an increase in the optical power of the TA. Above a seed power of 30mW the TA is saturated and the power can't increase furthermore. Note that the TA can work several

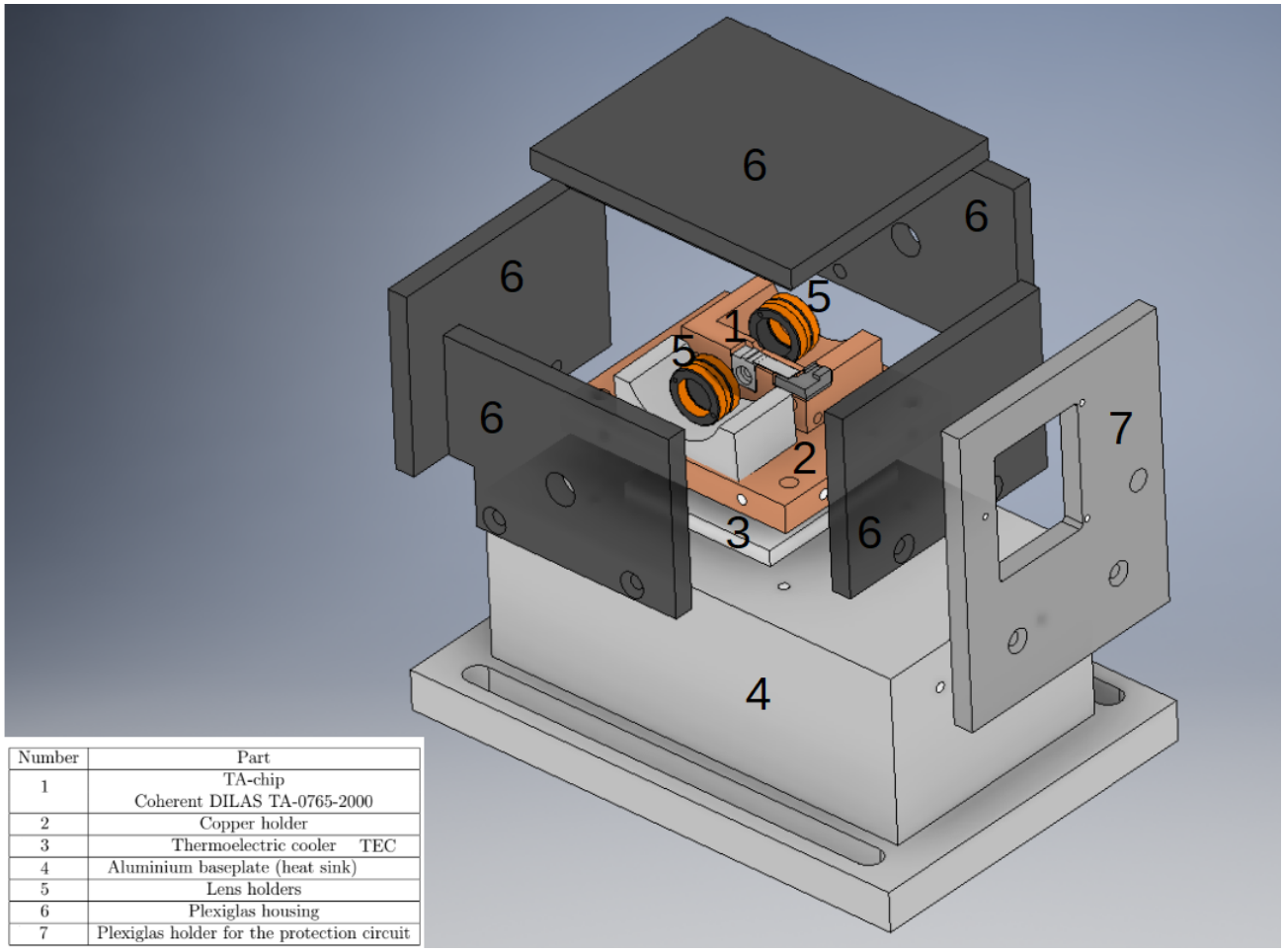

Number	Part
1	TA-chip Coherent DILAS TA-0765-2000
2	Copper holder
3	Thermoelectric cooler TEC
4	Aluminium baseplate (heat sink)
5	Lens holders
6	Plexiglas housing
7	Plexiglas holder for the protection circuit

Figure 4.26: Sketch of the TA system assembly

hours without optical injection at Max.current 2A. On the other hand, seeding the TA without electrical power might leads to damage in the TA-chip, because the TA acts in this case like a photo-diode and builds up charges on its leads that can electrocute it [21]. The TA output can be also increased roughly by increasing the operation current as illustrated in Fig.4.30. Be careful not to exceed 4.5A!. All measurements plotted in Fig.4.29,4.30 and 4.31 were taken directly before the optical isolator.

4.3.5 Coupling the TA-beam into a single-mode optical fiber

The TA output beam is coupled into a single-mode optical fiber to improve its beam quality, where the single mode fiber acts as a spatial mode filter. It should be noted that the coupling efficiency is not constanst when changing the TA current, because the beam-profile changes when the output power changes and as a result the coupling efficiency will change. The reason for that is because changing the TA current leads to change in the index of refraction of the gain medium, which changes the astigmatism of the beam [21].

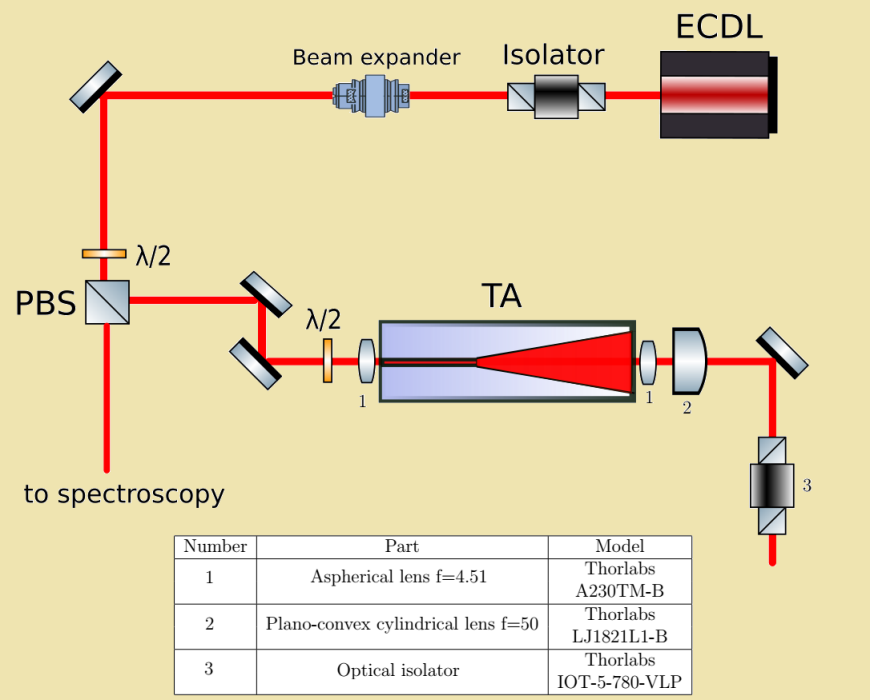

Number	Part	Model
1	Aspherical lens f=4.51	Thorlabs A230TM-B
2	Plano-convex cylindrical lens f=50	Thorlabs LJ1821L1-B
3	Optical isolator	Thorlabs IOT-5-780-VLP

Figure 4.27: Optical path of coupling the seed laser into the TA and collimating the TA output. A half waveplate is used to tun the seed light polarization and consequently tuning the TA output power. The optical isolator is important to prevent any back reflection, which can cases damaging of the TA chip. The measured transmission through the optical isolater is about 75% at 770nm.

That's why the coupling efficiency was optimized at high output power, at which the TA will operate later during the experiment. The mode profile corresponded to the highest coupling efficiency were recorded by a beam imaging camera (BladeCam-HR) before and after fiber coupling at high output power and hence high current I_{TA}=4A as shown in Fig.4.32. It's obvious that the TA beam quality is very poor and as was promised the beam becomes nearly Gaussian after fiber coupling. Two adjustable mirrors have been used to couple the light into the fiber, which provide two degrees of freedom and an aspherical lens f=7.5 is used to focus the light into the fiber in cage system, where the position of the lens is adjustable (see Table4.1). The focal length is calculated from the formula: $f = \frac{\pi dD}{4\lambda}$ where d is the beam diameter, D is the mode field diameter and λ is the wavelength. In our case $D = 4.5\mu$m, $d \approx 1.685$mm and $\lambda = 770$nm.
A coupling efficiency of 50% has been achieved at current 4A and we got an optical power of 600 mW after the single-mode fiber.

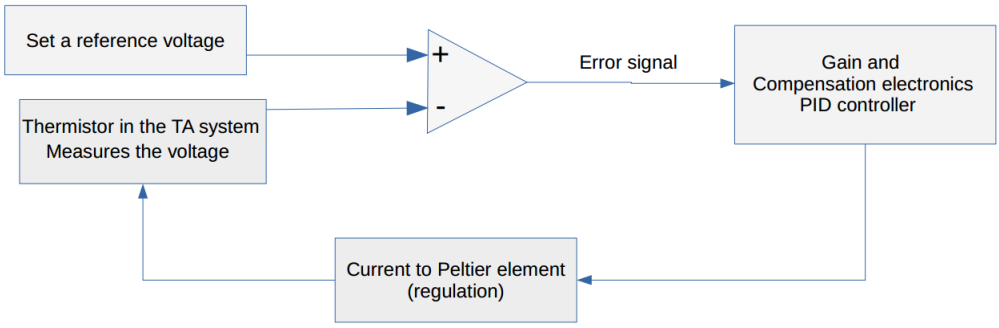

Figure 4.28: the principle working of the PID-temprature regulator of the TA, adapted from [29]

Part	model
Z-Axis Translation Mount, 30 mm Cage Compatible	Thorlabs SM1Z
Aspheric Lens f=7.50 mm	Thorlabs A375TM-B
Fiber Adapter Plate	Thorlabs SM1FCA
30 mm Cage Plate for the aspheric lens	Thorlabs CP1TM09/M

Table 4.1: Components of the fiber coupler

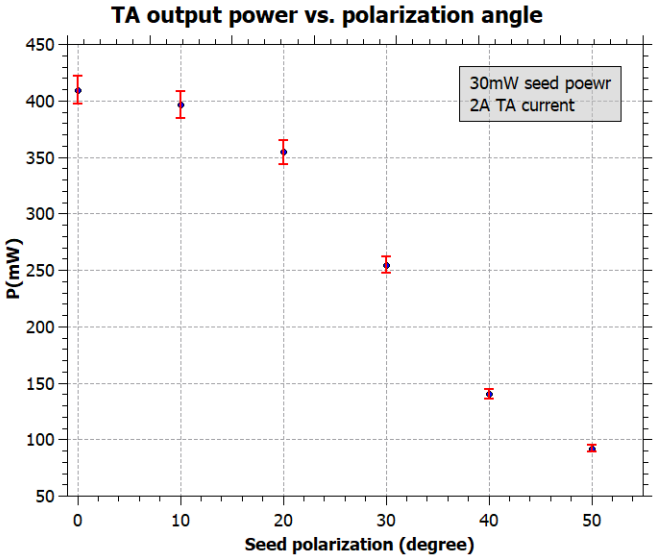

Figure 4.29: TA output power versus the polarization angle of the seed beam at fixed TA current and seed power. Maximum TA optical power for transverse magnetic (TM) polarized seed laser beam. By rotating the seed polarization 50° the power can be decreased to 22.5% of it's maximum value.

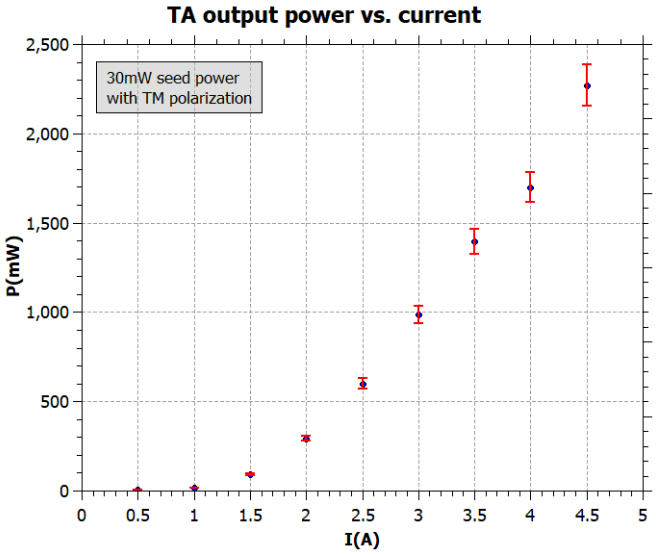

Figure 4.30: TA output power as a function of the driving current at constant optical injection power and polarization. Above 1.5A the TA power increases linearly with increasing the current. The Maximum TA output power is 2.27(11)W at maximum current 4.5A, maximum seed power 30mW and TM polarization.

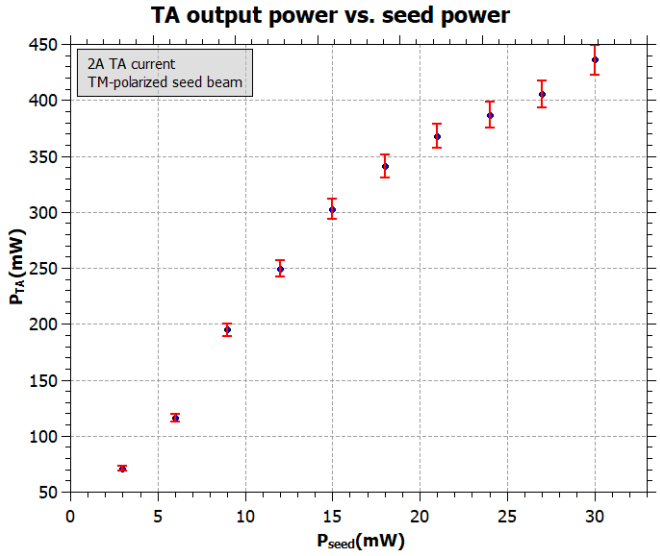

Figure 4.31: Dependence of TA output power on the seed power at fixed operation current and seed polarization.

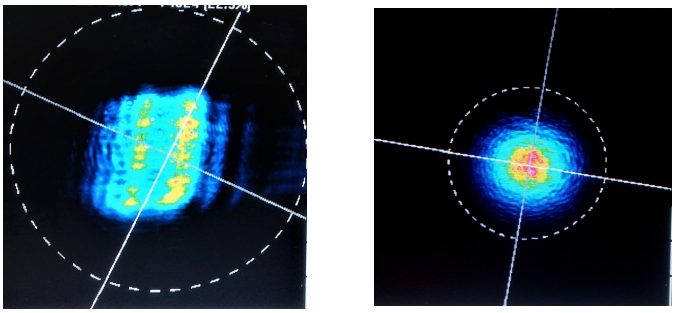

(a) (b)

Figure 4.32: The TA beam profile before and after fiber coupling: (a) poor beam quality at a distance 62cm from the output facet, the major and minor diameter are 2.04mm and 1.33mm, respectively. (b) nearly Gaussian mode after fibre coupling (mean diameter 1.07mm with a collimating lens f=11mm)

4.4 Generating the cooling and repumping frequencies

The laser frequency is locked to the crossover frequency ω_{c2}, which has to be shifted down to generate the cooling frequency ω_C and up to generate the repumping frequency ω_R with blue detuning $\delta_C = \delta_R$ from the atomic resonances $F = 2 \rightarrow F' = 2$ for the cooling beam and $F = 1 \rightarrow F' = 2$ for the repumping beam.

$$\omega_C = \omega_{c2} - \underbrace{\frac{461.7}{2} + \delta_C}_{2\Omega_C} \tag{4.27}$$

$$\omega_R = \omega_{c2} + \underbrace{\frac{461.7}{2} + \delta_R}_{2\Omega_R} \tag{4.28}$$

where $2\Omega_c$ and $2\Omega_R$ are the required shifts to produce the cooling and repumping frequencies, respectively. These frequency shifts can be obtained by means of two acousto-optic modulators (AOMs) in double pass configuration.
This section introduce our double-pass acousto-optic modulator system. First we start with the principle working of the AOM. We move then to describe how to control the AOM RF-signal. Next we present the experimental setup of the system and its characteristic features. Finally, fiber couplings of the cooling and repumping beams are performed and the corresponding coupling efficiencies are reported.

4.4.1 Acousto-optic modulator (AOM)

A propagated sound wave inside an optical medium can modulate its refractive index creating gradient in the index of refraction and consequently changing the optical effect of the medium on light passing through it. This acousto-optic effect can be seen classically as a Bragg scattering (Bragg reflection) of light by set of successive wavefronts spaced by the acoustic wavelength Λ, as illustrated in Fig.4.33 .The sound wave acts like a diffraction grating and constructive interference occurs only when the Bragg condition is satisfied:

$$2\Lambda \sin\theta = m\lambda \tag{4.29}$$

where λ the wavelength of light in the medium $\lambda = \lambda_0/n$, λ_0 the wavelength of light in vacuum, n the refractive index, and m integer number (order of diffraction).
This Light-sound interaction can be treated in quantum physics as photon-phonon interaction. It is a scattering process, where photons scattered by phonons. Let's consider an incident photon in an optical wave of wavevector $\mathbf{k_1}$ and angular frequency ω_1 interacts with phonon of wavevector $\mathbf{q}$ and angular frequency Ω. This interaction generates a new photon in a diffracted beam of wavevector $\mathbf{k_2}$ and angular frequency ω_2. Energy and

momentum are conserved in the process, meaning:

$$\hbar\omega_2 = \hbar\omega_1 \pm \hbar\Omega \tag{4.30}$$

$$\hbar\mathbf{k_2} = \hbar\mathbf{k_1} \pm \hbar\mathbf{q} \tag{4.31}$$

the first equation represents a Doppler shifting:

$$\omega_2 = \omega_1 \pm \Omega \tag{4.32}$$

and the second equation can be written as:

$$\mathbf{k_2} = \mathbf{k_1} \pm \mathbf{q} \tag{4.33}$$

which is equivalent to the Bragg condition $2\Lambda \sin\theta = \lambda$
The sign plus and minus indicates whether the generated photon upshifted or downshifted in frequency, respectively. Upshifted Bragg scattering requires absorbing phonon, while downshifted Bragg scattering requires generating phonon.

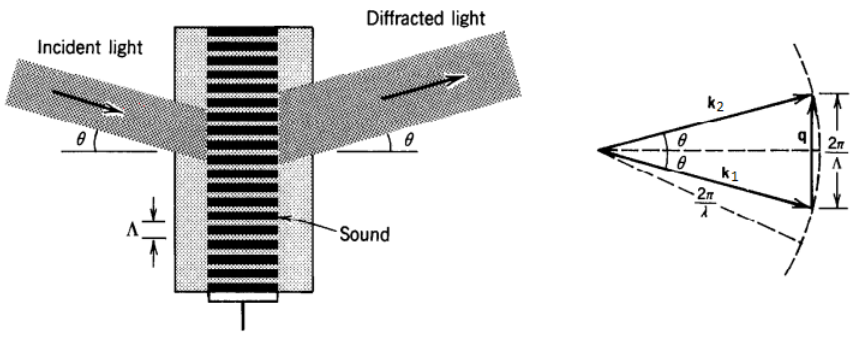

Figure 4.33: Acousto-optic effect. An incident light wave with a wavelength λ and angular frequency ω_1 is upshiffted and diffracted from a sound wave, its wavelength is Λ with angular frequency Ω. The angular frequency of the diffracted light is $\omega_2 = \omega_1 + \Omega$. Bragg condition is fulfilled when $\theta = \frac{\lambda}{2\Lambda}$. The Vector relation diagram of the momentum conservation $\mathbf{k_2} = \mathbf{k_1} + \mathbf{q}$ is illustrated to the right. [33]

Our AOM is designed for a RF signal with frequency $f_c = 110$MHz and bandwidth of 50 MHz. The crystal made of TeO_2 and the incidence Bragg angle is 10 mrad at the center frequency modulation for propagating light with wavelength 770 nm.

4.4.2 RF signal control

RF driver is used to supply the AOM by RF-signal. The driver consists of a Voltage Controlled Oscillator (VCO) and Voltage Variable Attenuator (VVA). The VCO generates a sinusoidal wave, whose frequency can be tuned linearly by tuning the applied

voltage. Our VCO has a typical sensitivity 7-10 MHz/V [27]. The function of the VVA is to attenuate the output power of the VCO signal. The level of attention can be controlled by varying the applied voltage. The output power of the signal provided by the RF-driver (P_{max}=5.6 dBm) is not enough to drive the AOM, therefore a separated high power amplifier is used. Our amplifier has a minimum output power of +33 dBm [26]. One should be careful not to exceed the maximum accepted RF power by the AOM, which is according to the AOM-datasheet 2.2 W=33.4 dBm. The amplifier is connected to the RF-driver by SMA cable. The cable has to be as short as possible to reduce any loss of the signal or generating of noise [24]. The safety sequence for connecting is as following: 1-connect the amplifier to the AOM via SMA cable. 2-apply DC voltage on the amplifier(24 V). 3-connect the RF-driver to a voltage source (±30 V). And for disconnecting from 3 to 1.
It should be noted that the amplitude and the frequency of the RF signal can be adjusted not only manually from the AOM driver but also digitally using LabVIEW based graphical user interface.

4.4.3 Double-pass acousto-optic modulator system

The diffraction angle of the beam depends on the modulation frequency Ω of the AOM. It's desired therefore to use the AOM in a double pass arrangement to prevent this dependency when tuning the AOM-frequency [11]. Otherwise, The alignment has to be fixed each time to maintain the coupling efficiency when the laser beam is coupled into a fibre.
In the first pass the zero order is blocked, while the first order is focused by a lens onto a mirror in cat's eye configuration (see Fig.4.34). The laser beam is then retroreflected to the AOM after being collimated by the lens. In the second pass the first order is deflected and the zero order has to be blocked. The total frequency shift after the second pass is twice the modulation frequency. Using a quarter wave plate and polarization beam splitter (PBS) one can separate the double pass laser beam from the original beam. A sketch of our double-pass acousto-optic modulator system is illustrated in Fig.4.35.

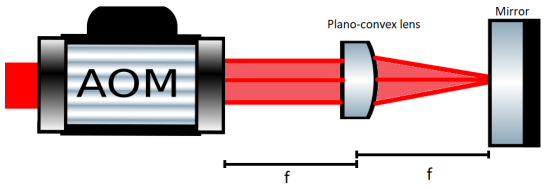

Figure 4.34: A cat's eye retroreflector is placed at the focal point of plano convex lens. The reflected laser beam has the same radius after being collimated by the lens. The distance between the lens and the AOM is also equal to the focal length.

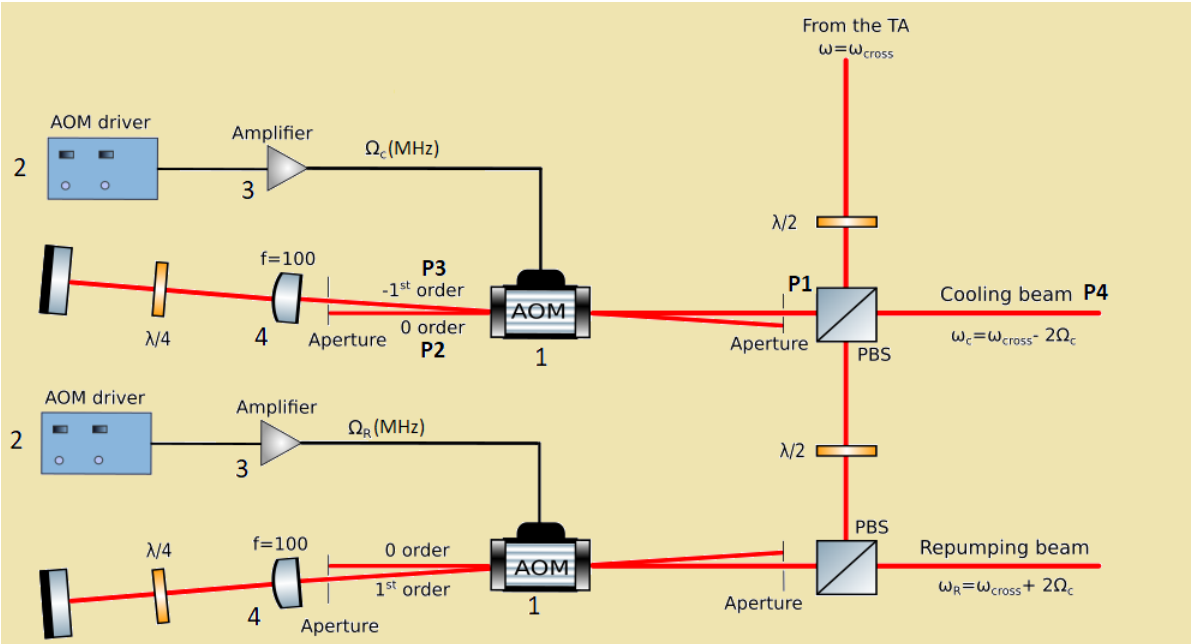

number	Part		Model
1	Acousto-optic modulator the center frequency $f_c = 110$ MHz		Opto-electronic MT110-A1.5-IR
2	AOM driver includes	Voltage-Controlled Oscillator (VCO) $100 - 200$ MHz	Mini-Circuits ZX95-200-S+
		Voltage Variable Attenuator (VVA)	Mini-Circuits ZX73-2500-S+
3	High Power Amplifier		Mini-Circuits ZHL-1-2W-S+
4	Plano-Convex Lens f=100		Thorlabs LA1509-B

Figure 4.35: Double-pass acousto-optic modulator system for generating the cooling and repumping beams with a description of the optical and electronic components used in the construction.

4.4.4 Performance of the system

The characteristic parameters of the system can be defined as following [24]:
Diffraction efficiency $= P_3/P_2$
Single pass efficiency $= P_3/P_1$
Double pass efficiency $= P_4/P_1$
Transmission $= P_2/P_1$
where P_1 the optical power of the beam before passing the AOM. P_2 the optical power of the zero order beam when the AOM is switched off, P_3 the optical power of the first order beam after the first pass and P_4 is the optical power of the douple-pass beam as shown in Fig.4.35. In the Tab.4.2 stand those for generating cooling and repumping beams with positive detuning $\delta_C = \delta_R = 3.5\Gamma$.
It should be noted that the diffraction efficiency depends on the RF signal power and the

	Cooling beam	Repumping beam
Diffraction efficiency	75.3%	85.6%
Single pass efficiency	73%	83%
Double pass efficiency	56%	65%
Transmission	97%	97%

Table 4.2: the characteristic properties of the double-pass acousto-optic modulator system for generating cooling and repumping beams with blue detuning $\delta_C = \delta_R = 3.5\Gamma = 2\pi \times 21\text{MHz}$.

	Cooling beam	Repumping beam
Coupling efficiency	84%	75%

Table 4.3: Coupling efficiency of the cooling and repumping beams into a single mode fiber

angle of incidence. Thus, the diffraction efficiency can be optimized by alignment and by increasing the RF-power. However, increasing the RF power more than an optimum value leads to decreasing in the efficiency.

4.4.5 Coupling the cooling- and repumping beams into a fiber

After the double pass we couple the cooling and repumping beams each into a single mode fiber with focusing lens f=11mm. The measured coupling efficiencies are reported in Tab4.3. [1]
At this point we have finished building the D1-laser system and we come to the conclusion in the next chapter.

[1]The total outcome optical power of the system after fiber coupling at 4A operation current of the TA is about 287mW, which is higher than the required optical power for gray molasses cooling.

Chapter 5

Conclusion

In this thesis, we have presented the experimental setup of a laser system for sub-Doppler cooling on the D1 transition of ^{39}K atoms. As shown in Fig.5.1 we have used a low power laser diode in external cavity and interference filter as a wavelength selection element at 770nm. The laser frequency has been successfully stabilized in the short- (laser linewidth in KHz range) and long term (no frequency drift over 12 hours) to one of the atomic features of the D1 line using frequency modulation (FM) technique. The optical output power has been amplified from the mW to W range by means of tapered amplifier (TA). For optimizing the quality of the TA beam profile, the TA output beam has been coupled into a single mode fiber with 50% coupling efficiency at high optical power ($I_{TA} = 4$A). Finally we shift the frequency by two acousto-optic modulatores (AOMs) in double pass configuration to introduce the required cooling- and repumping beams and we coupled each into a single mode fiber.
It remains important for future work to build and implement a laser system for cooling sodium atoms on the D1 transition, so we can renounce the evaporative cooling of Sodium atoms in the main chamber of our current experiment.

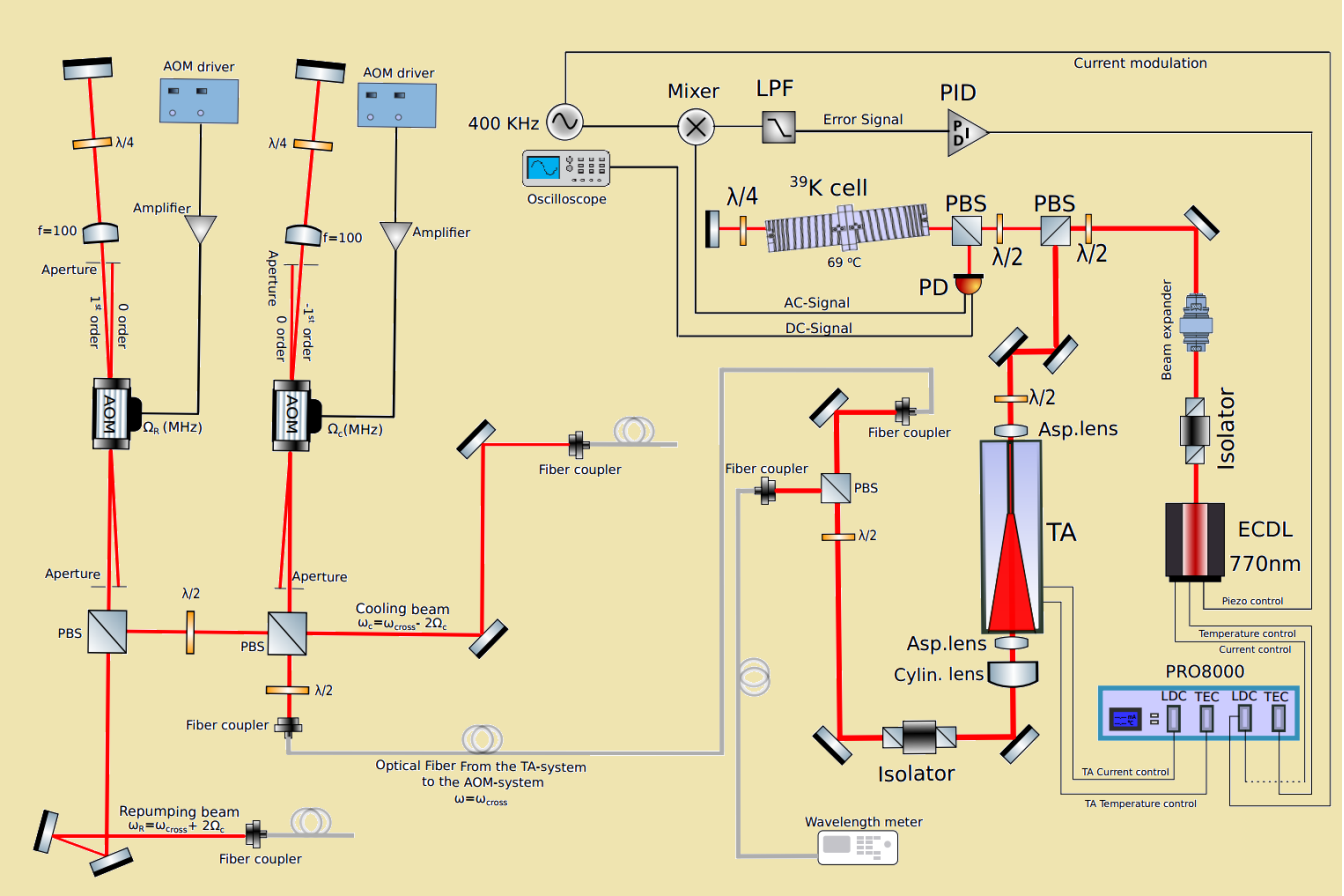

Figure 5.1: Illustration of the ^{39}K D1 laser system including all optical and electronic components and devices.

Bibliography

[1] A. Aspect, E. Arimondo, R. e. a. Kaiser, N. Vansteenkiste, and C. Cohen-Tannoudji. Laser cooling below the one-photon recoil energy by velocity-selective coherent population trapping. *Physical Review Letters*, 61(7):826, 1988.

[2] X. Baillard, A. Gauguet, S. Bize, P. Lemonde, P. Laurent, A. Clairon, and P. Rosenbusch. Interference-filter-stabilized external-cavity diode lasers. *Optics Communications*, 266(2):609–613, 2006.

[3] G. C. Bjorklund, M. Levenson, W. Lenth, and C. Ortiz. Frequency modulation (fm) spectroscopy. *Applied Physics B*, 32(3):145–152, 1983.

[4] I. Bloch, J. Dalibard, and W. Zwerger. Many-body physics with ultracold gases. *Reviews of modern physics*, 80(3):885, 2008.

[5] L. A. Coldren, S. W. Corzine, and M. L. Mashanovitch. *Diode lasers and photonic integrated circuits*, volume 218. John Wiley & Sons, 2012.

[6] J. Dalibard and C. Cohen-Tannoudji. Laser cooling below the doppler limit by polarization gradients: simple theoretical models. *JOSA B*, 6(11):2023–2045, 1989.

[7] K. B. Davis, M.-O. Mewes, M. R. Andrews, N. Van Druten, D. Durfee, D. Kurn, and W. Ketterle. Bose-einstein condensation in a gas of sodium atoms. *Physical review letters*, 75(22):3969, 1995.

[8] C. D'Errico, M. Zaccanti, M. Fattori, G. Roati, M. Inguscio, G. Modugno, and A. Simoni. Feshbach resonances in ultracold 39k. *New Journal of Physics*, 9(7):223, 2007.

[9] R. D. Diehl and R. L. Diehl. *High-power diode lasers: fundamentals, technology, applications*, volume 78. Springer Science & Business Media, 2000.

[10] C. . DILAS. Tapered amplifier for mopa setups ta-0765-2000. `http://dilas.com/assets/media/products/DILAS_TA-0765-2000.pdf`, 2017.

[11] E. A. Donley, T. P. Heavner, F. Levi, M. Tataw, and S. R. Jefferts. Double-pass acousto-optic modulator system. *Review of Scientific Instruments*, 76(6):063112, 2005.

[12] C. Dornes and A. Dorn. *3D-focusing Spectrometer for a Reaction Microscope*. PhD thesis, Ruprecht-Karls-Universität Heidelberg, Germany, 2011.

[13] eagleyard Photonics. Gallium arsenide semiconductor laser diode eyp-rwe-0780-02000-1300-sot12-0000. `https://www.xsoptix.com/data/eagleyard/Datasheets/ds_EYP-RWE-0780-02000-1300-SOT12-0000.pdf`.

[14] D. R. Fernandes, F. Sievers, N. Kretzschmar, S. Wu, C. Salomon, and F. Chevy. Sub-doppler laser cooling of fermionic 40k atoms in three-dimensional gray optical molasses. *EPL (Europhysics Letters)*, 100(6):63001, 2012.

[15] C. J. Foot et al. *Atomic physics*, volume 7. Oxford University Press, 2005.

[16] C. Fort, A. Bambini, L. Cacciapuoti, F. Cataliotti, M. Prevedelli, G. Tino, and M. Inguscio. Cooling mechanisms in potassium magneto-optical traps. *The European Physical Journal D-Atomic, Molecular, Optical and Plasma Physics*, 3(2):113–118, 1998.

[17] M. Fox. *Quantum optics: an introduction*, volume 15. OUP Oxford, 2006.

[18] E. Gehrig, O. Hess, C. Seibert, D. Woll, and R. Wallenstein. Amplification and wave mixing of induced and spontaneous emission in semiconductor laser amplifiers. *Applied Physics B*, 76(3):285–288, 2003.

[19] M. Gerken. *Gray Molasses Cooling of Lithium-6 Towards a Degenerate Fermi Gas*. Master's thesis, University of Heidelberg, Germany, 2016.

[20] G. E. Hall and S. W. North. Transient laser frequency modulation spectroscopy. *Annual review of physical chemistry*, 51(1):243–274, 2000.

[21] J. C. Kangara, A. J. Hachtel, M. C. Gillette, J. T. Barkeloo, E. R. Clements, S. Bali, B. E. Unks, N. A. Proite, D. D. Yavuz, P. J. Martin, et al. Design and construction of cost-effective tapered amplifier systems for laser cooling and trapping experiments. *American Journal of Physics*, 82(8):805–817, 2014.

[22] P. D. Lett, W. D. Phillips, S. Rolston, C. E. Tanner, R. Watts, and C. Westbrook. Optical molasses. *JOSA B*, 6(11):2084–2107, 1989.

[23] K. Macadam and A. Steinbach. Saturated absorption spectroscopy experiment sas.

[24] D. McCarron. A guide to acousto-optic modulators. 2007.

[25] P. Melentiev, M. Subbotin, and V. Balykin. Simple and effective modulation of diode lasers. *LASER PHYSICS-LAWRENCE-*, 11(8):891–896, 2001.

[26] Mini-Circuits. High power amplifier zhl-1-2w-s(+). `https://ww2.minicircuits.com/pdfs/ZHL-1-2W.pdf`, 2019.

[27] Mini-Circuits. Voltage controlled oscillator zx95-200+. https://ww2.minicircuits.com/pdfs/ZX95-200+.pdf, 2019.

[28] D. Nath, R. K. Easwaran, G. Rajalakshmi, and C. Unnikrishnan. Quantum-interference-enhanced deep sub-doppler cooling of 39 k atoms in gray molasses. *Physical Review A*, 88(5):053407, 2013.

[29] G. P. Nyamuda. *Design and development of an external cavity diode laser for laser cooling and spectroscopy applications*. PhD thesis, Stellenbosch: University of Stellenbosch, 2006.

[30] F. Papoff, F. Mauri, and E. Arimondo. Transient velocity-selective coherent population trapping in one dimension. *JOSA B*, 9(3):321–331, 1992.

[31] L. Pollet, J. Picon, H. Büchler, and M. Troyer. Supersolid phase with cold polar molecules on a triangular lattice. *Physical review letters*, 104(12):125302, 2010.

[32] D. W. Preston. Doppler-free saturated absorption: Laser spectroscopy. *American Journal of Physics*, 64(11):1432–1436, 1996.

[33] B. E. Saleh, M. C. Teich, and B. E. Saleh. *Fundamentals of photonics*, volume 22. Wiley New York, 1991.

[34] G. Salomon, L. Fouché, P. Wang, A. Aspect, P. Bouyer, and T. Bourdel. Gray-molasses cooling of 39k to a high phase-space density. *EPL (Europhysics Letters)*, 104(6):63002, 2014.

[35] M. Scholl et al. Interference filter stabilized external cavity diode laser. *Ultra Cold Atoms Lab, Department of Physics, University of Toronto, Canada*, 2010.

[36] T. A. Schulze. *Quantum degenerate mixtures of 23Na-39K and coherent transfer paths in NaK molecules*. PhD thesis, Hannover: Institutionelles Repositorium der Leibniz Universität Hannover, 2018.

[37] Schäfter+Kirchhoff. Anamorphic beam-shaping optics 5an. https://www.sukhamburg.com/products/Anamorphic_beam-shaping_Optics_5AN.html.

[38] F. Stubenrauch. Frequency modulation saturation spectroscopy laser lock of an interference-filterstabilized external-cavity diode laser. Technical report, Research report, University of Toronto, 2010. 69, 2010.

[39] H. Sun. *A practical guide to handling laser diode beams*. Springer, 2015.

[40] M. Tarnowski. *Implementation and characterization of a gray molasses and of tunable hexagonal optical lattices for 40K*. Master's thesis, Universität Hamburg, Germany, 2015.

[41] Thorlabs. Gc25075-k - potassium borosilicate reference cell, Ø25 mm x 71.8 mm. https://www.thorlabs.de/thorproduct.cfm?partnumber=GC25075-K.

[42] T. Tiecke. Properties of potassium. *University of Amsterdam, The Netherlands, Thesis*, pages 12–14, 2010.

[43] A. G. Truscott, K. E. Strecker, W. I. McAlexander, G. B. Partridge, and R. G. Hulet. Observation of fermi pressure in a gas of trapped atoms. *Science*, 291(5513):2570–2572, 2001.

[44] J. Walpole. Semiconductor amplifiers and lasers with tapered gain regions. *Optical and Quantum Electronics*, 28(6):623–645, 1996.

[45] M. Weidemüller, T. Esslinger, M. Ol'Shanii, A. Hemmerich, and T. Hänsch. A novel scheme for efficient cooling below the photon recoil limit. *EPL (Europhysics Letters)*, 27(2):109, 1994.